Year: 2024

Myeloid-T cell interplay and cell state transitions associated with checkpoint inhibitor response in melanoma
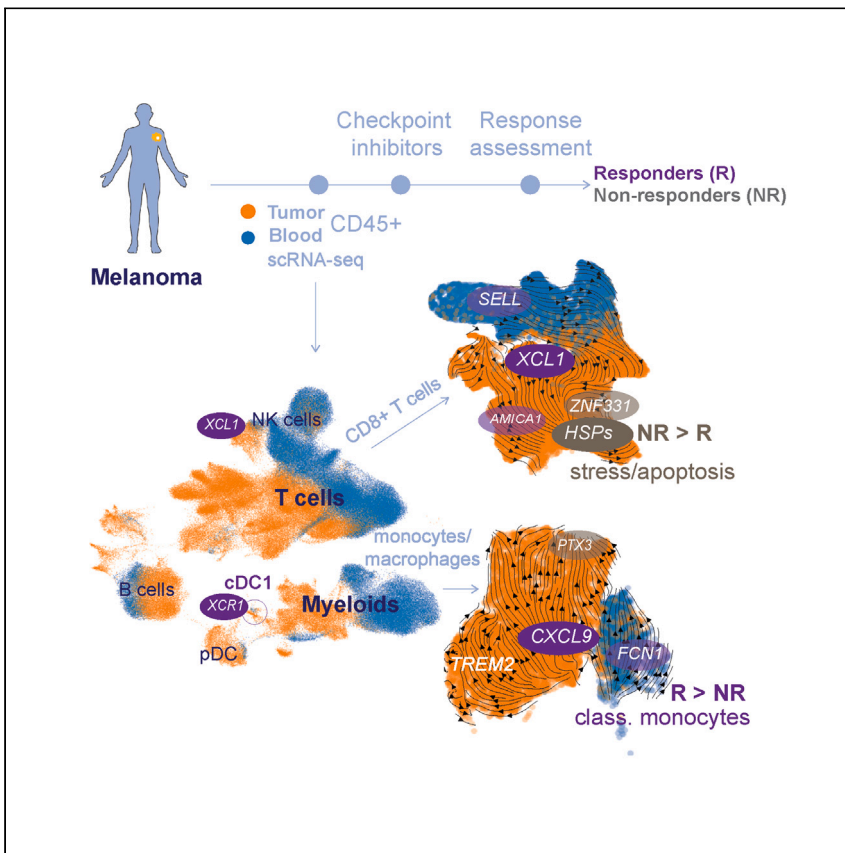
Schlenker, Ramona ; Schwalie, Petra C ; Dettling, Steffen ; Huesser, Tamara ; Irmisch, Anja ; Mariani, Marisa ; Martínez Gómez, Julia M ; Ribeiro, Alison ; Limani, Florian ; Herter, Sylvia ; Yángüez, Emilio ; Hoves, Sabine ; Somandin, Jitka ; Siebourg-Polster, Juliane ; Kam-Thong, Tony ; de Matos, Ines Grazina ; Umana, Pablo ; Dummer, Reinhard ; Levesque, Mitchell P ; Bacac, Marina

Med

Article

Myeloid-T cell interplay and cell state transitions associated with checkpoint inhibitor response in melanoma

Schlenker et al. generate a high-resolution immune cell atlas of metastatic melanoma tumors and peripheral blood using single-cell RNA sequencing. They relate the baseline immune cell contexture to response to checkpoint inhibitor therapy, characterizing distinct myeloid, T, and NK cell state transitions and putative interactions across response classes.

Translation to Patients

Ramona Schlenker, Petra C. Schwalie, Steffen Dettling, ..., Reinhard Dummer, Mitchell P. Levesque, Marina Bacac

ramona.schlenker@roche.com (R.S.)
petra.schwalie@roche.com (P.C.S.)

Highlights

Immune cell atlas of melanoma lesions and peripheral blood prior to immunotherapy

Monocytes are enriched in responders and transition into $CXCL9^+$ macrophages

Non-responder-enriched myeloid-T/NK cell interactions are primarily immunosuppressive

Non-responder $CD8^+$ T cells progress into a state of stress, apoptosis, and hypoxia

Med

 CellPress

Article

Myeloid-T cell interplay and cell state transitions associated with checkpoint inhibitor response in melanoma

Ramona Schlenker,[1,5,7,*] Petra C. Schwalie,[2,5,*] Steffen Dettling,[1] Tamara Huesser,[3] Anja Irmisch,[4] Marisa Mariani,[3] Julia M. Martínez Gómez,[4] Alison Ribeiro,[3] Florian Limani,[3] Sylvia Herter,[3] Emilio Yángüez,[3] Sabine Hoves,[1] Jitka Somandin,[3] Juliane Siebourg-Polster,[2] Tony Kam-Thong,[2] Ines Grazina de Matos,[3] Pablo Umana,[3] Reinhard Dummer,[4] Mitchell P. Levesque,[4,6] and Marina Bacac[3,6]

SUMMARY

Background: The treatment of melanoma, the deadliest form of skin cancer, has greatly benefited from immunotherapy. However, many patients do not show a durable response, which is only partially explained by known resistance mechanisms.

Methods: We performed single-cell RNA sequencing of tumor immune infiltrates and matched peripheral blood mononuclear cells of 22 checkpoint inhibitor (CPI)-naive stage III–IV metastatic melanoma patients. After sample collection, the same patients received CPI treatment, and their response was assessed.

Findings: CPI responders showed high levels of classical monocytes in peripheral blood, which preferentially transitioned toward *CXCL9*-expressing macrophages in tumors. Trajectories of tumor-infiltrating CD8^{+} T cells diverged at the level of effector memory/stem-like T cells, with non-responder cells progressing into a state characterized by cellular stress and apoptosis-related gene expression. Consistently, predicted non-responder-enriched myeloid-T/natural killer cell interactions were primarily immunosuppressive, while responder-enriched interactions were supportive of T cell priming and effector function.

Conclusions: Our study illustrates that the tumor immune microenvironment prior to CPI treatment can be indicative of response. In perspective, modulating the myeloid and/or effector cell compartment by altering the described cell interactions and transitions could improve immunotherapy response.

Funding: This research was funded by Roche Pharma Research and Early Development.

CONTEXT AND SIGNIFICANCE

There is an unmet need for deciphering cancer immunotherapy response-predicting factors and understanding mechanisms leading to treatment resistance. Researchers from Roche Pharma Research and Early Development and the University Hospital of Zurich have sequenced tumor and blood samples of melanoma patients before they received checkpoint inhibitor treatment. They have identified differences between patients responding and not responding to treatment, including distinct immune cell frequencies, differentiation states, and putative cell-cell interactions. Modulating the described patterns could improve the response to checkpoint inhibitors.

INTRODUCTION

Rates of melanoma, the deadliest form of skin cancer, have been continuously rising over the past decades.[1] Cutaneous melanomas originate in melanocytes and are typically associated with UV light exposure and high immunogenicity.[2] This is underscored by a high abundance of neoantigens,[3] the existence of melanoma-responsive tumor-infiltrating lymphocytes (TILs), and the efficacy observed upon TILs transfer in clinical trials.[4] The engagement of melanoma-specific T cells by immune checkpoint

⌀ CellPress

Med
Article

blockade and subsequent clinical benefit led to the approval of the anti-CTLA4 antibody ipilimumab in 2011 for metastatic melanoma,[5,6] followed by the anti-PD1 antibodies pembrolizumab and nivolumab in 2014.[1,2,7–10] Subsequently, the combination of nivolumab with ipilimumab or the LAG-3-targeting antibody re-latlimab has been shown to induce stronger long-term efficacy compared with monotherapy.[1,11–13]

Despite these advances, 42% of stage III and IV melanoma patients remain unresponsive to the ipilimumab/nivolumab combination, and 66% show disease progression within 6.5 years,[11] creating the need for a better understanding of cancer immunotherapy (CIT) response-predicting factors and mechanisms underlying therapy resistance.[2] Recent studies have used the increased resolution provided by single-cell RNA sequencing (scRNA-seq) to more deeply characterize cell populations and states in the tumor microenvironment likely to affect CIT response and resistance.[14–20] Most studies have revealed that the majority of tumor-infiltrating CD8^{+} T cells show high expression of exhaustion and/or cytotoxicity markers.[14–18] Recently, a TCF1^{+} PD1^{+} subpopulation (termed stem-like T cells) has been proposed to be one of the key tumor-reactive CD8^{+} T cell populations giving rise to terminally differentiated T cells upon CPI treatment.[15,21–24] In melanoma, the relative fraction of TCF1^{+} CD8^{+} cells was found to be elevated in CIT responders,[15,21–24] suggesting that a higher pool of responsive CD8^{+} T cells may be beneficial. However, we still have a limited understanding of the relation between this cell population and effector T cells detected in peripheral blood. In addition, the relation between effector T cells and myeloid cell populations, crucial for T cell priming and inhibition by secreting inhibitory signals, has been poorly explored.

To address these points, we performed scRNA-seq analysis of the CD45^{+} immune cell fraction of metastatic melanoma lesions and matched peripheral blood samples of CPI-naive stage III–IV patients. These patients received CPI treatment after sample collection, and we monitored their clinical response. Our study reveals cell state transitions of peripheral blood and tumor-derived immune cells as well as putative cellular interactions and their association with response to CPI treatment.

RESULTS

Immune cell heterogeneity in tumor tissue and peripheral blood of metastatic melanoma patients

We performed scRNA-seq of immune cells isolated from surgically resected metastatic or primary tumor lesions of stage III–IV CPI treatment-naive melanoma patients (n = 22) and their corresponding peripheral blood mononuclear cells (PBMCs) (available for 20 patients) (Table S1, study cohort). The metastatic lesions stemmed from lymph nodes (n = 11), brain (n = 5), lung (n = 1), and subcutaneous metastases (n = 4), and one lesion was from a primary melanoma (n = 1). After surgery, patients received CPI treatment (n = 3 a-CTLA-4, n = 13 a-PD1, n = 5 a-CTLA-4 + a-PD1, and n = 1 a-LAG3 + a-PD1) in the adjuvant setting (n = 13, no evidence of disease after surgery) and non-adjuvant setting (n = 9, patients had remaining lesions post-surgery) (Figure 1A). Responders (R) were defined as patients who showed signs of clinical benefit, including partial and complete response, or remained tumor free (TF) 6 months after treatment initiation. Non-Rs (NRs) were defined as patients who showed signs of progression within the first 6 months after CPI treatment. The final scRNA-seq cohort consisted of 134,986 tumor-infiltrating and 114,537 peripheral blood CD45^{+} immune cells derived from 9 TF, 3 R, 8 NR (n = 3 adjuvant, n = 5 non-adjuvant), and 2 non-classified patients (STAR Methods).

[1]Roche Innovation Center Munich, Roche Pharma Research and Early Development (pRED), Penzberg, Germany

[2]Roche Innovation Center Basel, pRED, Basel, Switzerland

[3]Roche Innovation Center Zurich, pRED, Schlieren, Switzerland

[4]Department of Dermatology, University Hospital Zurich, University of Zurich, Zurich, Switzerland

[5]These authors contributed equally

[6]Senior author

[7]Lead contact

*Correspondence:
ramona.schlenker@roche.com (R.S.),
petra.schwalie@roche.com (P.C.S.)

https://doi.org/10.1016/j.medj.2024.03.015

Med
Article

CellPress

Given that increased tumor mutational burden (TMB) has been previously positively associated with CIT response,[25] we also assessed TMB in our cohort. We observed a trend for higher median TMB in the R group, while the difference was not significant (Figure S1A; $p \geq 0.1$ for all R vs. NR comparisons). Given the limited cohort size, this result is in line with previous reports, as TMB alone is unlikely to explain the difference in clinical outcome.

Joint unsupervised clustering of the CD45$^+$ immune cell fraction from tumor lesions and peripheral blood resulted in distinct separation of lymphocytes of the B lineage, T cells, natural killer (NK) cells, and myeloid cells (Figure 1B), irrespective of their lesion of origin, tumor mutation status (BRAF vs. NRAS), response, or other variables (Figures 1B and S1B). For each of these major immune cell types, we identified specific subpopulations characterized by unique marker gene expression patterns (STAR Methods; Table S2; Figures S1C and S1D): 4 B lymphocyte types (naive, memory, germinal center B cells, and plasma cells), 15 T cell types (naive, memory, effector, cytokine/chemokine-expressing, exhausted-like, proliferating T cells, and regulatory, cytotoxic/NK-like T cells among the CD4 and/or CD8 subsets), 3 NK cell types (CD56-dim, CD56-bright, and proliferating NK cells), 5 dendritic cell (DC) subtypes (cDC1/CD141$^+$ conventional DC [cDC], cDC2/CD1c$^+$ cDCs, activated/CCR7$^+$ cDCs, immature DCs, and plasmacytoid DCs [pDCs]), 2 monocyte types (classical and non-classical), 3 macrophage subtypes (M2-like: *MARCO$^+$/SPP1$^+$* tumor-associated macrophage [TAM], *MSR1$^+$/ C1QC$^+$/TREM2$^+$* TAMs, M1-like: *CXCL9$^+$/CXCL10$^+$/ISG15$^+$* TAMs, and a patient-specific group with mixed characteristics, which we did not further subclassify) (Figure 1C).

Comparing immune cells from blood and tumor lesions, we found large differences in their frequencies (Figures 1D and S1E; Table S3). For instance, cytokine-expressing CD56-bright NK cells; proliferating CD8$^+$, CD4$^+$ T cells; and exhausted-like and various effector and memory T cell subtypes were exclusively or predominantly found in tumors. Cytotoxic CD56-dim NK cells, cytotoxic/NK-like T cells, and naive T cells were mainly found in peripheral blood. B cells were, on average, detected at similar levels in tumor and blood, while plasma cells were more frequent in tumor lesions. With respect to the myeloid lineage, as expected, macrophages were only detected in tumors, while monocytes were the predominant myeloid population in the peripheral blood. Various types of DCs, particularly CD141$^+$ (cDC1) and CCR7$^+$ (activated) DCs, were strongly enriched in tumors compared with peripheral blood.

Similarly, while all cell subtypes were detected in most individuals, there was high variability of the relative cell type frequency among individuals, in particular within TILs (Figure S2A). To explore how the observed heterogeneity relates to factors such as individual age, gender, mutation status, CPI response, or tissue of origin (lesion), we summarized single-cell data per sample (creating pseudo-bulk profiles), performed principal-component analysis (PCA), and correlated the main components with metadata information (STAR Methods). We found that principal component 1 (PC1) strongly correlated with mutation status, as most BRAF$^+$ patients ($n = 10$) grouped separately from NRAS$^+$ patients ($n = 7$) (Figure S2B). BRAF$^+$ samples showed an enrichment of (naive) B cells and (naive) CD4$^+$ T cells, while mature CD8$^+$ subtypes were overrepresented in NRAS$^+$ samples (Figures 1F–1H and S2C–S2E; Tables S3 and S4). However, the majority of BRAF$^+$ samples originated from lymph nodes, which also tended to show higher B and naive CD4$^+$ T cell fractions, as expected. A larger cohort would be required to delineate the main driver of the observed differences.
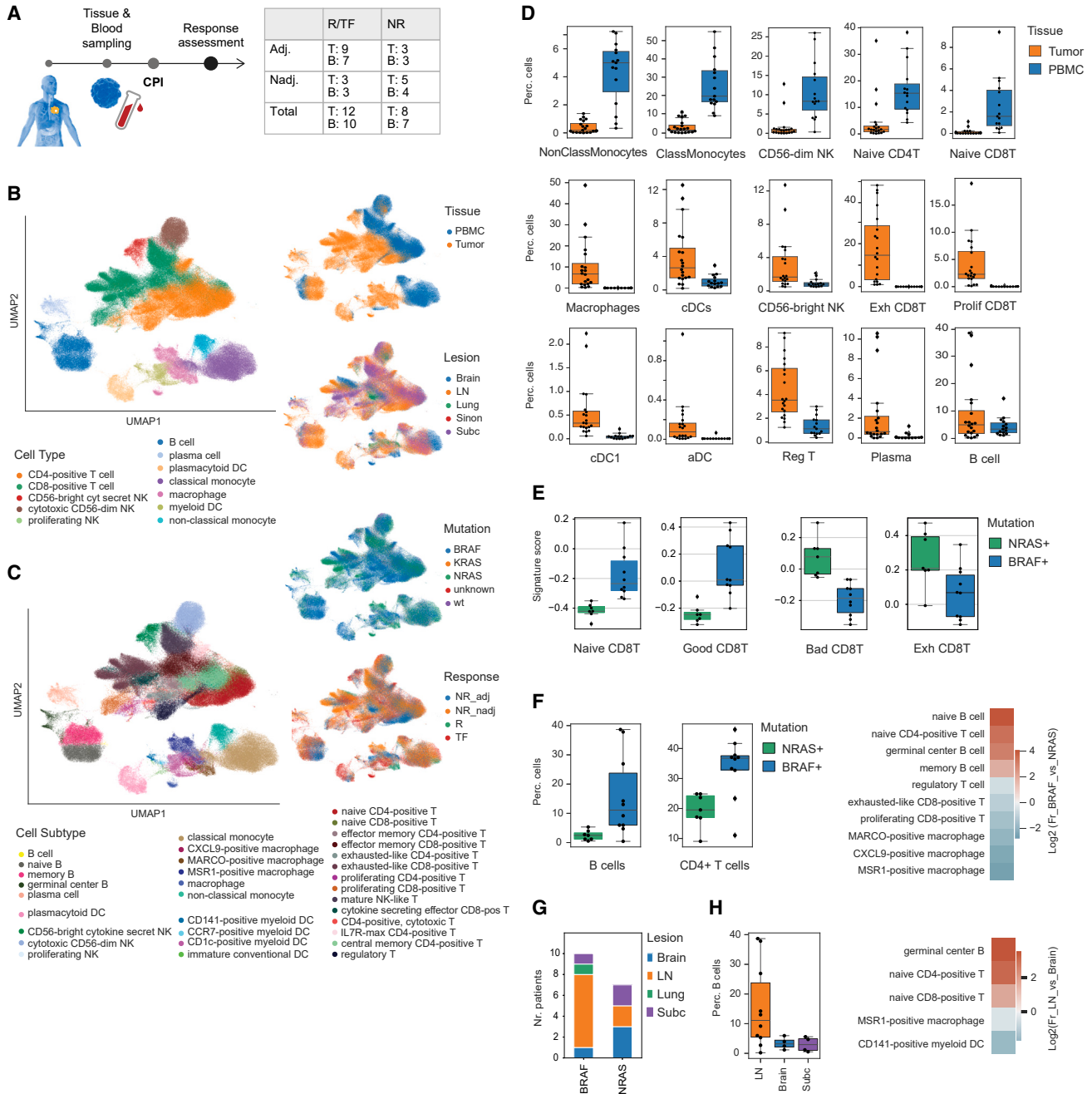
Figure 1. Immune cell heterogeneity in tumor tissue and peripheral blood of metastatic melanoma patients

(A) Overview of the study setup and cohort size of checkpoint inhibitor (CPI)-naive tissue (T) and blood samples (B) and the response classes: adjuvant (Adj) and non-adjuvant (Nadj); R, responder; TF, tumor free; NR, non-responder.

(B and C) 2D UMAP visualization of all CD45+ cells across both PBMCs and tumor tissue, colored according to main cell type (B) and subtype (C), sampling location (tissue), lesion of origin (LN, lymph node; Subc, subcutaneous; Sinon, sinonasal), patient mutation (WT, wild type), and CPI response status (response).

(D) Percentage (Perc.) of selected cell types in PBMCs versus tumor samples across all patients.

(E–G) BRAF- vs. NRAS-mutated sample comparison.

(E) Signature scores for selected differentially enriched T cell-related signatures (Exh, exhausted).

(F) Left: percentage of selected cell types. Right: overview of fraction (Fr) of cell type ratio (BRAF vs. NRAS).

(G) Number (Nr.) of patients stratified by mutation and lesion of origin.

(H) Left: percentage of B cells across main lesions of origin. Right: overview of fraction (Fr) of cell type ratios in LN vs. brain samples.
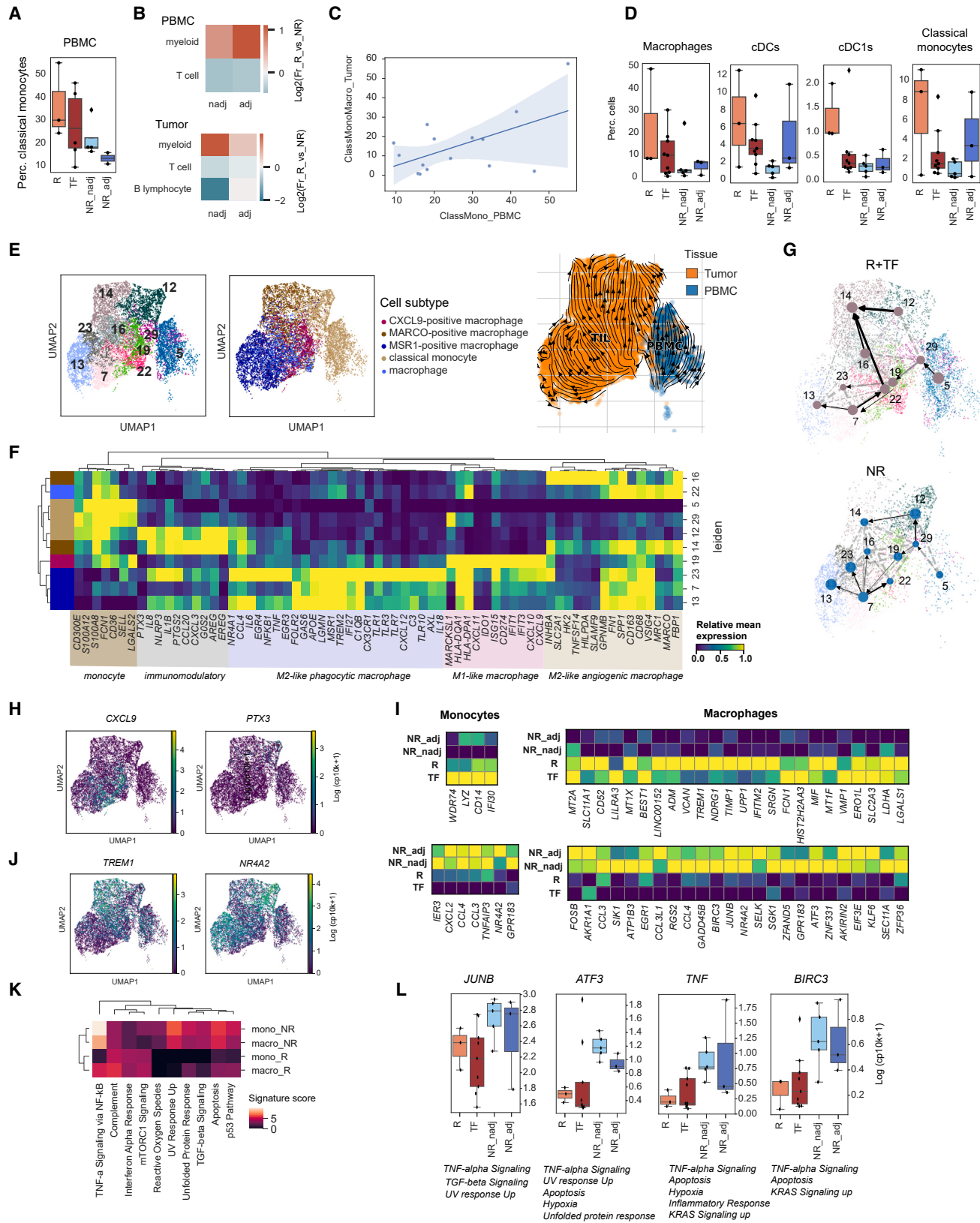
Figure 2. Monocytes of CPI Rs preferentially transition toward *CXCL9*-expressing macrophages

(A–C) Comparison of relative cell frequencies across response classes: Adj and Nadj.

(A) Percentage (Perc.) of classical monocytes among PBMCs (R+TF vs. NR: *p* = 0.04).

(B) Overview of fraction of main cell type ratio in PBMCs (top) and tumor (bottom).

(C) Fraction of classical monocytes per sample in PBMCs (x axis) vs. fraction of classical monocytes and macrophages in tumor tissues (Pearson's r = 0.55, *p* = 0.03).

(D) Percentage of selected myeloid subpopulations stratified according to response classes (significant differences: cDC1 R+TF vs. NR, *p* = 0.03; R vs. NR_nadj, *p* = 0.01).

(E) UMAP visualization of transitional classical monocytes and macrophages from both tumor and PBMC samples colored according to Leiden cluster number (left), cell subtype (center), and sampling location (right). Tumor (TIL, tumor-infiltrating lymphocyte), orange; PBMC, blue. Right: velocity vectors are projected on the UMAP (streamline plot, where similarly directed vectors are connected).

(F) Relative (standardized column-wise) mean expression of selected marker genes across the clusters and subpopulations shown in (E).

(G) PAGA-estimated transitions between myeloid clusters stratified by response (edge thickness corresponds to transition confidence).

(H) *CXCL9* and *PTX3* expression overview as representative marker genes for clusters 19 and 12, respectively.

(I) Relative (standardized column-wise) mean expression of genes significantly and consistently differentially expressed, separated by response classes (R/TF-enriched, top; NR-enriched, bottom) in monocytes (left) and macrophages (right).

(J) *TREM1* and *NR4A2* expression overview as representative R- and NR-enriched genes, respectively.

(K) Signature scores for Hallmark pathways significantly enriched in R or NR monocytes (mono) and/or macrophages (macro).

(L) Expression of selected genes involved in the pathways shown in (K), summarized per sample and response class. Corresponding selected pathway memberships are also displayed.

CPI R monocytes preferentially transition toward *CXCL9*-expressing macrophages

We next examined the relation between immune composition and CPI response. Consistent with data published by Krieg et al.,[26] we detected a higher frequency of classical monocytes in the blood of CPI R/TF patients compared with NRs (mean R/TF: 36%/28% vs. NR: 21%/13%, *p* = 0.041; Figures 2A and S3A; Table S3). In addition, R/TF patients showed higher proportions of myeloid cells in both tumor and peripheral blood (Figure 2B). Interestingly, patients with the highest proportion of classical monocytes in PBMCs also showed the highest relative fraction of classical monocytes/macrophages in the tumor, revealing a positive correlation between peripheral blood and tumor tissue (Pearson's r = 0.55, *p* = 0.03; Figure 2C). Moreover, in tumor lesions, we also detected a higher frequency of cDC1s (CD141$^+$ myeloid DCs) (mean R/TF: 1.3%/0.6% vs. NR: 0.3%/0.3, *p* = 0.028) and a lower frequency of exhausted-like CD4$^+$ T cells (mean R/TF: 1%/2.9% vs. NR: 7%/2.8%, *p* = 0.032) in R/TFs compared with NRs (Figures 2D and S3A–S3C). In the non-adjuvant cohort, we further detected a higher frequency of myeloid DCs (mean R: 6.8% vs. NR: 1.2%), macrophages (mean R: 21.8% vs. NR: 6.5% NR), pDCs (R: 1.7% vs. NR: 0.7%), and classical monocytes (R: 6.8% vs. NR: 0.9%) in Rs (all *p* < 0.05). In contrast, germinal center B cells and plasma cells were enriched in NRs (*p* < 0.01).

Further exploring the characteristics of the myeloid compartment and delving into the putative relations between cell subtypes, we performed joint clustering, trajectory, and velocity analyses[27–30] (Figure S3D; STAR Methods). Classical monocytes were predicted to transition into macrophages, consistent with the widely accepted model of monocyte differentiation into macrophages upon tissue entry[31] (Figures 2E and S3D). This transition occurred via a cluster of classical monocyte-like cells present in both blood and tumor (Figure 2E, cluster 29), characterized by high expression of *S100A8/12*, *CD36*, *MARCKSL1*, *SELL*, and *CD300E* (Figure 2F; Table S4), genes previously associated with inflammation, activation, and migration.[32–42]

Next, we inspected macrophage marker gene expression, considering both classical *in vitro* M1 versus M2 classification[43] and more recent complex phenotypes revealed by *ex vivo* scRNA-seq experiments.[44–48] We identified M1-like chemokine-expressing (*CXCL9/10/ISG15$^+$*, type I interferon high, cluster 19), M2-like phagocytic (*MSR1/C1QC/TREM2/FOLR2$^+$*, clusters 7 and 13), and M2-like angiogenic

Med
Article

 CellPress

(*MARCO/SPP1/PPARG/VEGFA*⁺, clusters 14, 16, and 22) macrophages, a group of cells that retained monocyte-specific expression and upregulated immune-regulatory markers and showed relatively low major histocompatibility complex (MHC)-related expression (cluster 12), and finally a group with mixed phenotypes (cluster 23; Figures 2E and 2F). Velocity and partition-based graph abstraction (PAGA) analysis suggested that transitional monocytes (cluster 29) gave rise to either *CXCL9*-expressing macrophages (cluster 19) or, specifically in the NR tumors, to the immune-regulatory monocyte-like cells (cluster 12). In addition, in Rs, the terminal angiogenic macrophage population (cluster 14) primarily arose from macrophage populations with a similar phenotype (clusters 16 and 22) and not only from the monocyte-like population (Figures 2G and 2H).

We also found significantly higher expression of markers associated with activation, such as *TREM1*, *LYZ*, *FCN1*, and *IFITM2*, with a strong enrichment of type I interferon, complement, and mTORC1 signaling pathways in macrophages and monocytes of Rs (Figures 2I–2K; Tables S4 and S5). In contrast, NRs showed highest *CXCL2*, *CCL3/4*, and *CCL3L1* expression, enrichment of transforming growth factor β (TGF-β) signaling, apoptosis, unfolded protein response, and tumor necrosis factor alpha (TNF-α) signaling, also exemplified by high expression of *JUNB*, *ATF3*, *TNF*, and *BIRC3* (Figures 2I–2L; Tables S4 and S5).

In summary, we found high relative fractions of circulating classical monocytes and tumor-infiltrating monocytes/macrophage in R/TF patients and identified a transmigratory cell population estimated to preferentially transition into M1-like macrophages in R/TF patients. This suggests a putative increased migration and activation potential of peripheral monocytes in tumors of R patients.

CPI response associates with distinct myeloid-T/NK cell interactions

Myeloid cell populations can shape the tumor microenvironment by providing pro- or anti-inflammatory signals to effector cells, including CD8⁺, CD4⁺ T cells, and NK cells. We thus investigated whether myeloid populations were estimated to preferentially interact with specific T/NK subsets, using CellphoneDB[49] (STAR Methods). We calculated putative interactions per cell type pair separately per patient and selected interactions more frequently occurring in either R/TF patients or NRs that involved genes with expression enriched in the cell type of interest (STAR Methods). We found that NR samples were typically enriched in interactions involved in suppressing T cell responses, including TNFRSF10B-TNFSF10 (apoptosis),[50] TNF-VSIR/TNFRSF1B/TNFRSF1A/FAS (T cell inhibition and apoptosis),[51–53] TNFRSF1A-GRN (apoptosis),[51–53] and P2RY6-NAMPT (immunosuppression and M2 polarization),[54] among others. In contrast, R/TF-enriched monocyte/macrophage-T/NK interactions have been shown previously to positively influence effector cell activation: ICAM1-ITGAL/aLb2 complex (cell migration and lymphocyte activation)[55,56] and CD58⁻CD2 (T/NK activation and support of cytotoxicity)[57,58] (Figure 3A).

Intrigued by the higher frequency of cDC1 in the tumors of R/TF patients (Figure 2D), we extended the CellPhoneDB analysis to myeloid DC subtypes. In R/TF patients, we found an enrichment of XCR1-XCL1 (chemotaxis of cross-presenting DCs),[59–61] ICAM1-ITGAL (cell migration and lymphocyte activation),[55,56] interleukin-15 (IL-15)–IL-15R (T cell maintenance and proliferation),[62] and TNFRSF14-BTLA (DC homeostasis and T cell checkpoint)[63] interactions. NRs showed enrichments of P2RY6-NAMPT (immunosuppression and M2 polarization)[54] and TNFRSF1A-GRN (apoptosis)[51–53] (Figure 3B). In summary, in R/TF patients, cDC-T cell interactions

Med
Article

CellPress
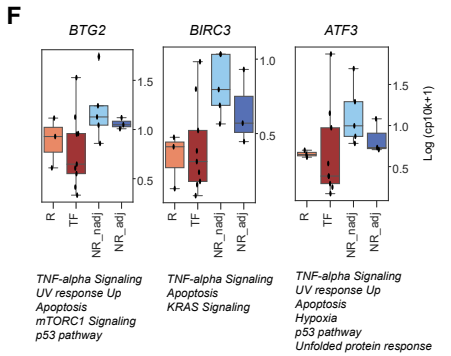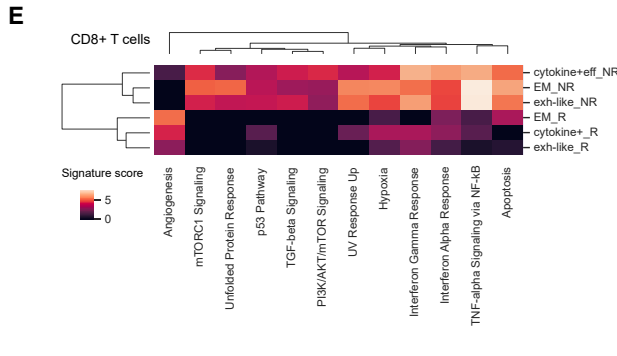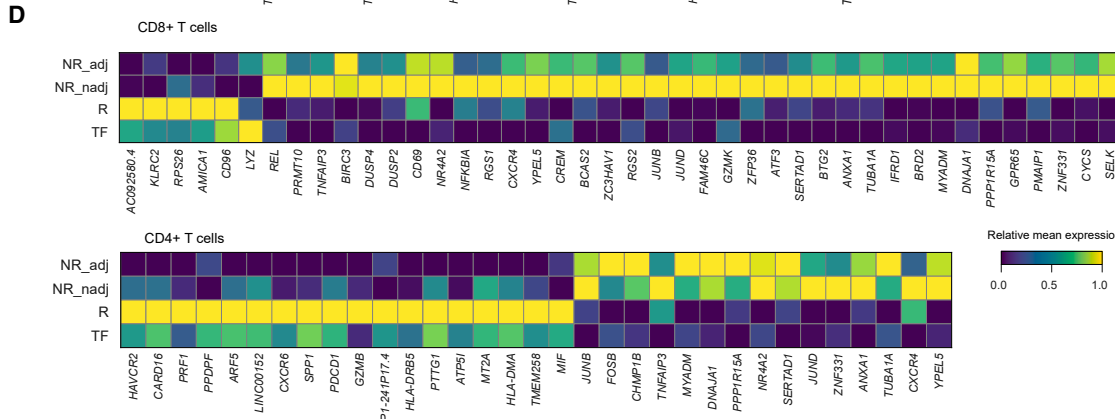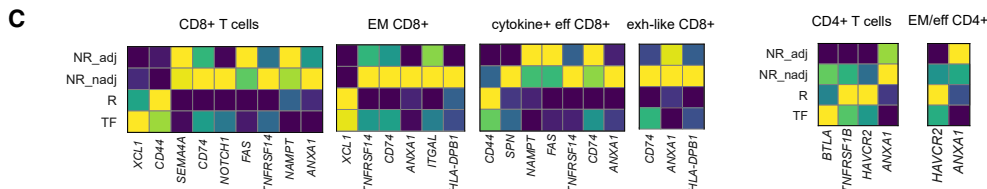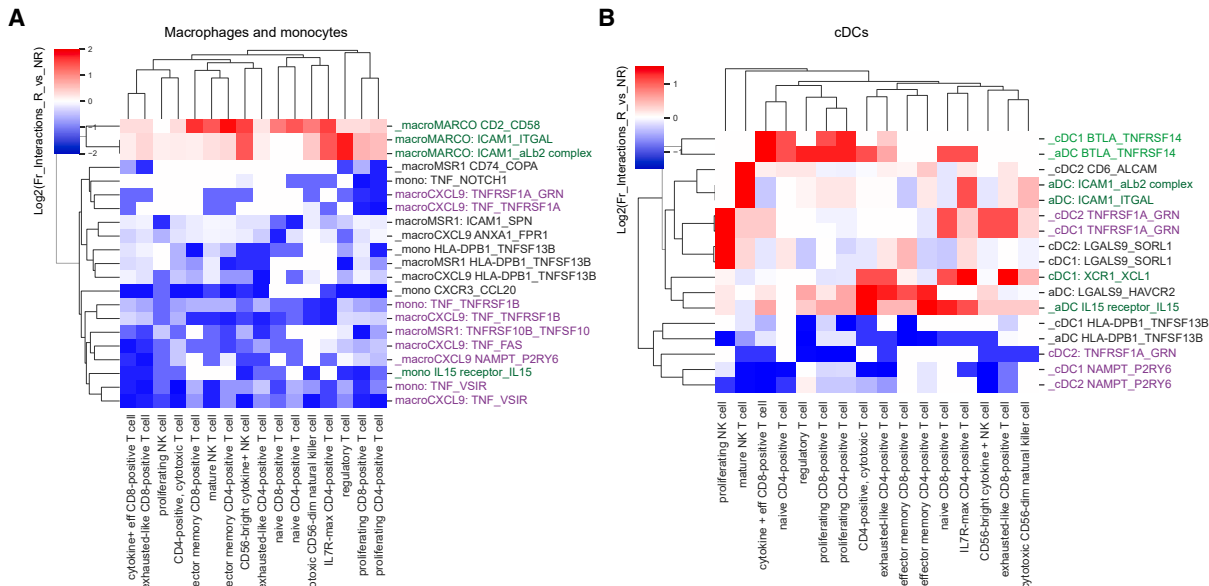
Figure 3. CPI response associates with distinct myeloid-T/NK cell interactions

(A and B) Ratio between the fractions of interactions predicted in R/TF vs. NR for (A) macrophages/monocytes and (B) cDC subtypes and CD8$^+$, CD4$^+$, and NK cell subsets (STAR Methods). Red, interactions occur more frequently in Rs; blue, in NRs; white, equal frequency. The first vs. second partner are separated by "_" for both cell types and genes. Genes previously positively (green) and negatively (purple) associated with T cell functionality are highlighted.

(C and D) Relative (standardized column-wise) mean expression of selected genes, summarized per response class for (C) interaction-involved genes that are also differentially expressed in the selected T cell subsets: effector memory (EM), cytokine-secreting effector (eff), and exhausted-like (exh-like) and (D) most stably and consistently differentially expressed genes (across tissues and response classes) among CD8$^+$ T cells (top) and CD4$^+$ T cells (bottom).

(E) Signature scores for Hallmark pathways significantly enriched in R or NR CD8$^+$ T cell subsets.

(F) Expression of selected genes that are members of the pathways shown in (E), summarized per sample and response class.

supporting T cell priming, activation, maintenance, and overall cell migration were more prevalent, while in NR patients, interactions involved in macrophage/monocyte-derived suppression of T cell response and induction of apoptosis were enriched.

We next assessed which genes estimated in preferential interactions were also significantly differentially expressed among response groups to gather additional evidence for their role and/or provide a rationale for the observed interaction bias. *CD44*, *BTLA*, *SELL*, *XCL1*, *HAVCR2*, and *TNFRSF1B* were significantly more highly expressed in CD4$^+$, CD8$^+$ T cells, or NK cells of R/TFs, consistent with a higher frequency of interactions they mediate (Figures 3C and S4A; Table S4). In contrast, *SEMA4A*, *NAMPT*, *FAS*, *ANXA1*, *ITGAL*, and others were more strongly expressed by effector cells of NRs (Figures 3C and S4A); with the exception of *ITGAL*, all of these genes were more frequently estimated to be mediating interactions with myeloid cells in NRs compared with Rs/TFs, further supporting their putative role in suppression of T cell functionality.

Finally, as some of these differentially expressed genes were cell type specific and only differed in the adjuvant/non-adjuvant setting or in specific lesions, we also asked which genes most consistently discriminated Rs/TFs from NRs (STAR Methods). Only a handful of genes were stably enriched in R/TF CD8$^+$ and NK cells, some of which have been shown previously to be involved in maintaining and enhancing T cell functionality and/or migration (e.g., *CD96*, *AMICA1*, and *KLRC2*) (Figures 3D and S4B).[64,65] Among R/TF-enriched genes in CD4$^+$ T cells were also *PDCD1*, *GZMB*, and *PRF1*, known markers of antigen experience and cytotoxicity. In contrast, we found a large number of genes to be consistently more highly expressed in NRs, including those known to negatively influence T cell response, such as *TNFAIP3*, *NFKBIA*, and *BTG2* (Figure 3D).[66] In line with the cell-cell interaction results, and similar to the macrophage analysis, genes more highly expressed in NR T cell subsets were related to apoptosis (*ATF3*, *BIRC3*, and *ANXA1*), TGF-β signaling (*TGIF1* and *PPP1R15A*), TNF-α signaling (*PPP1R15A*, *BTG3*, *BTG2*, *PLEK*, and *TNFAIP3*), or cellular response to stress (*DNAJA1* and *PMAIP1*), among others (Figures 3E, 3F, S4C, and S4D; Tables S4 and S5). Taken together, we found that functional and migratory T cell phenotypes were enriched in Rs/TFs, whereas those reflective of an apoptotic state were more prevalent in NR patients.

Trajectories leading to T cell dysfunction and cellular stress

To further understand the effector T cell compartment and the origin of the differentially expressed genes identified above, we jointly reanalyzed T cells from blood and tumor. We first performed joint clustering and trajectory analyses on CD4$^+$ T cells (Figures S5A–S5D) and then focused on memory and effector subsets for velocity and PAGA analyses (STAR Methods; Figures 4A–4F and S5). We found the main

directionality leading either from central memory (cluster 0) or from proliferating CD4^{+} T cells (cluster 9) toward effector memory T cells expressing markers of cellular stress (*HSPA1A*, *HSPA1B*, *ATF3*, cluster 5) (Figures 4C and 4D). When stratifying by response, while both Rs/TFs and NRs showed transitions from cluster 0 to 2 and 5 (central memory to effector memory/cellular stress), only NRs also showed a similarly strong transition from cluster 6 (effector) toward cluster 5. Strikingly, R/TF-enriched velocity driver genes were expressed across distinct CD4^{+} T cell subsets, including central memory (*ITGB1*), effector (*TIGIT*, *CXCR6*, and *CTLA4*), and proliferating (*BIRC5* and *TOP2A*) subsets. This was similar for the genes preferentially involved in myeloid-CD4^{+} T cell interactions in R/TF patients (Figures 4E and 4F; *BTLA*, *TNFRSF1B*, and *HAVCR2*). In contrast, NR-enriched velocity driver as well as interaction-involved genes tended to be most highly expressed in the most terminal, apoptotic-like cell state, corresponding to cluster 5 (*NR4A2*, *NFKBIA*, and *ANXA1*), putatively indicating a higher diversity of phenotypes in Rs/TFs vs. NRs.

The velocity analysis of the CD8^{+} T cell compartment identified the main directionality from naive and memory T cells toward the tumor-specific exhausted-like T cells (clusters 11, 5, 0, and 6), with cluster 10 (naive) estimated as initial and cluster 5 (exhausted) as the most terminal state (Figures 5A–5F; Figures S6A–S6D; Table S4). This is consistent with previous literature reports identifying an accumulation of "bad," exhausted-like, and cytotoxic CD8^{+} T cells in melanoma tumors[14,15,17] (Figure S6C). A first differentiation path linked naive cells via effector memory to activated and eventually exhausted-like T cells (clusters 10/16 to 3, 1, 9, and 0/11; Figures 5B–5D and S6A–S6D; orange in Figure 5E). A second path, specific to tumor-infiltrating CD8^{+} T cells, connected the pool of mature CD8^{+} T cells of cytokine-secreting (cluster 8), and proliferating (clusters 13 and 15) to the exhausted-like populations (Figures 5B–5D and S6A–S6D; purple in Figure 5E). Latent time estimations were in line with naive and effector memory cells being the earliest state (clusters 10, 16, 3, and 15), while exhausted-like cluster 5 cells were most terminal (Figures 5F and S6D). Cells in clusters 1, 13, 8, and 9 showed high heterogeneity of latent times, suggesting they may harbor transitioning cells, consistent with their positioning in the cluster connectivity graph. In addition, clusters 8 and 9, expressing *TCF7* and *PDCD1* but lacking *HAVCR2* (Figure 5B), transcriptionally resembled PD1^{+} TCF1^{+} stem-like CD8^{+} T cells, shown previously to undergo self-renewal and differentiation to terminally exhausted CD8^{+} T cells and to mediate the response to CPI therapy.[24]

Thus, a small subset of tumor-infiltrating CD8^{+} T cells with characteristics similar to CD8^{+} effector memory cells found in circulation as well as a subset of cytokine-secreting and/or proliferating CD8^{+} T cells appear to transition into distinct exhausted-like T cell populations in the tumors of melanoma patients. Interestingly, many genes noted above as preferentially involved in myeloid-T cell interactions in R/TF patients showed maximal expression in these naive/memory or transitional subsets (e.g., *SELL*, *XCL1*, and *BTLA*); in contrast, genes involved in NR-enriched interactions showed highest expression in the most terminal CD8^{+} T cell subsets (e.g., *HAVCR2*, *NAMPT*, *FAS*, and *SEMA4A*) (Figures 5B and 5G), further supporting the notion that the myeloid-T cell interplay may be involved in shaping T effector phenotypes.

NR CD8^{+} T cells are characterized by increased cellular stress and hypoxia

As less terminally differentiated CD8^{+} T cells have been associated previously with better patient outcome to CPI treatment,[4,15] we assessed the distribution of latent time values when stratifying across patients and response (Figure 6A). We found that, in the non-adjuvant setting, NRs tended to have larger latent time values

CellPress
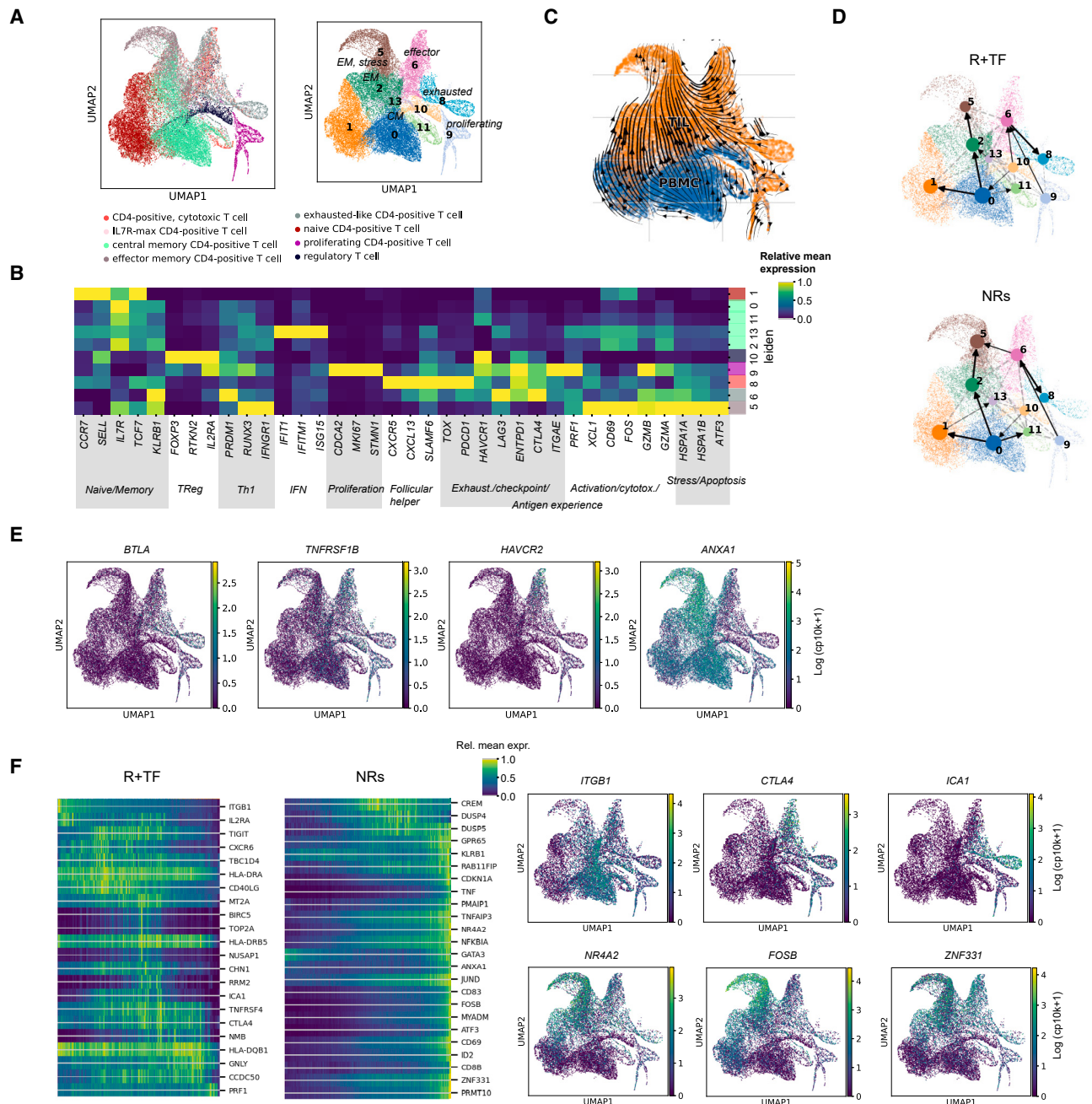
Figure 4. CD4+ T cell trajectories indicate increased transitions toward cellular stress in NRs

(A and B) UMAP visualization of CD4+ T cell subsets colored according to subtype (left) or Leiden clusters (right) (A) and relative (standardized column-wise) mean expression of selected marker genes across clusters (B).

(C) UMAP visualization of CD4+ T cell subsets colored according to sampling location: tumor (orange) and PBMC (blue). Estimated velocity vectors are projected on the UMAP.

(D) PAGA-estimated transitions between CD4+ T cell clusters (edge thickness corresponds to transition confidence), separated per response class.

(E) Expression of selected genes predicted to be frequently involved in myeloid-T cell interactions in R (*BTLA*, *TNFRSF1B*, *HAVCR2*) and NR (*ANXA1*).

(F) Left: relative (standardized row-wise) mean expression of velocity driver genes that are also differentially expressed in R/TF vs. NR patients, respectively. Cells are ordered (ascending) according to latent time estimation. Right: detailed view of the expression of selected heatmap genes in both categories (R/TF, top; NR, bottom).

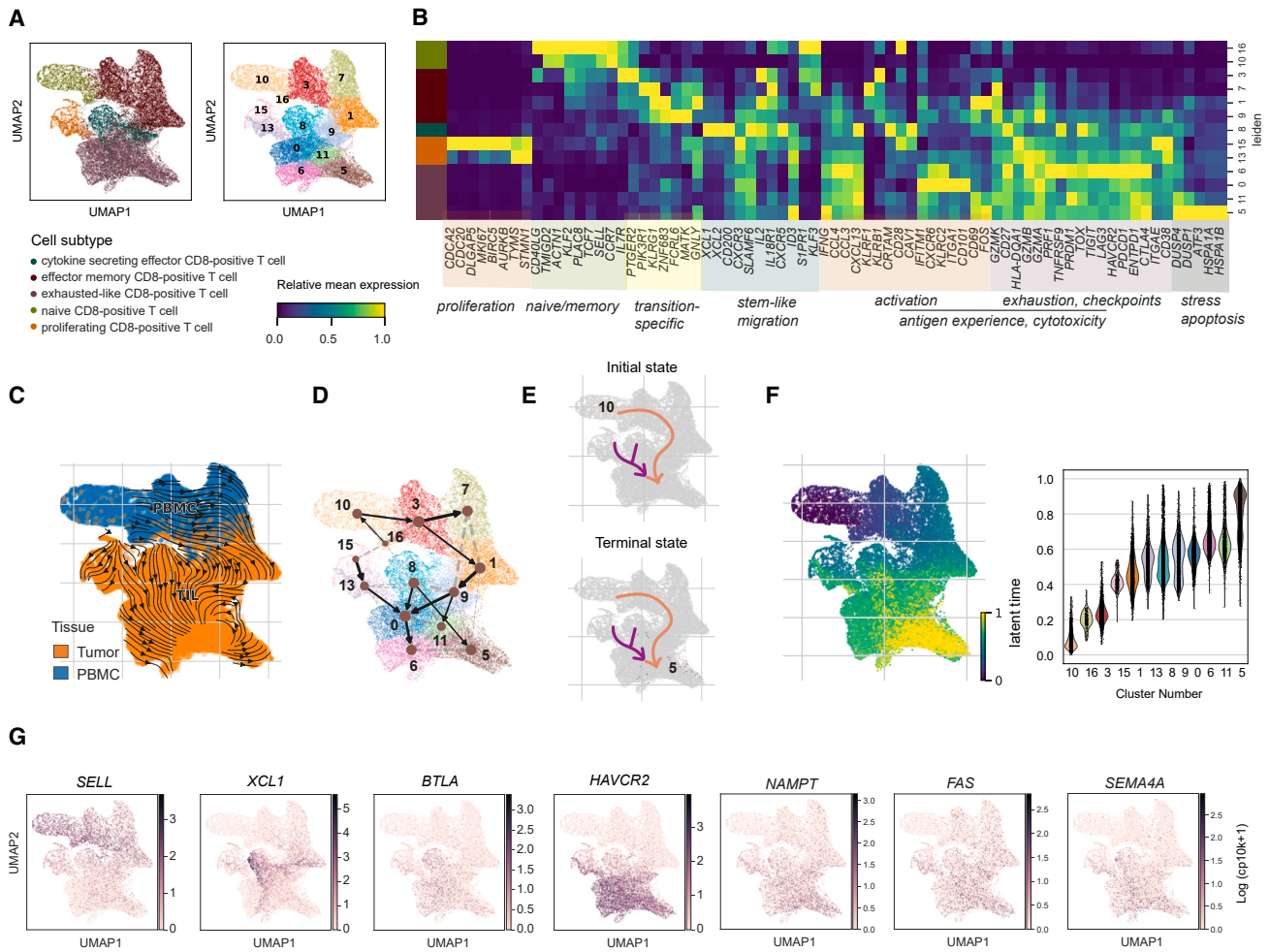**Figure 5. Velocity analysis revealed trajectories leading to CD8+ T cell terminal exhaustion**

(A) UMAP visualization of CD8+ T cell subsets colored according to subtype (left) or Leiden clusters (right).

(B) Relative (standardized column-wise) mean expression of selected marker genes across the clusters and subpopulations shown in (A).

(C) UMAP visualization of CD8+ T cell subsets colored according to sampling location: tumor (orange) and PBMC (blue). Estimated velocity vectors are projected on the UMAP (streamline plot, where similarly directed vectors are connected).

(D) PAGA-estimated transitions between CD8+ T cell clusters (edge thickness corresponds to transition confidence).

(E and F) Initial and terminal states (E) as well as cellular latent time estimates (F, left) for the trajectories shown in (C) and (D). Orange, naive to terminally exhausted; purple, proliferating and cytokine-secreting to exhausted-like and (F, right) latent time distribution per cluster.

(G) Expression of selected genes predicted to be frequently involved in myeloid-T cell interactions in R (SELL, XCL1, and BTLA) and NR (HAVCR2, NAMPT, FAS, and SEMA4A).

compared with Rs, in particular when considering cells of the heterogeneous transitional populations (clusters 8 and 9). The same trend was present among exhausted-like cells (Figures 6A and S6E), suggesting a more advanced state toward terminal differentiation of CD8+ T cells of NR. We next examined the differentiation trajectories in function of response and observed that, in Rs, most likely transitions were estimated toward clusters 0 and 6 (Figure 6B). In contrast, NR CD8+ T cells preferentially transitioned into clusters 11 and, ultimately, 5, which has been estimated previously as most terminal in the global analysis (Figure 6B).

To understand which pathways may underlie these differences, we examined velocity driver genes focusing on the transitions 9 to 11 and 13 to 11/5 in NRs and the transitions 9 to 0 and 8/13 to 0/6 in Rs/TFs (Figures 6C and S6G; STAR Methods). Our

Med
Article

CellPress
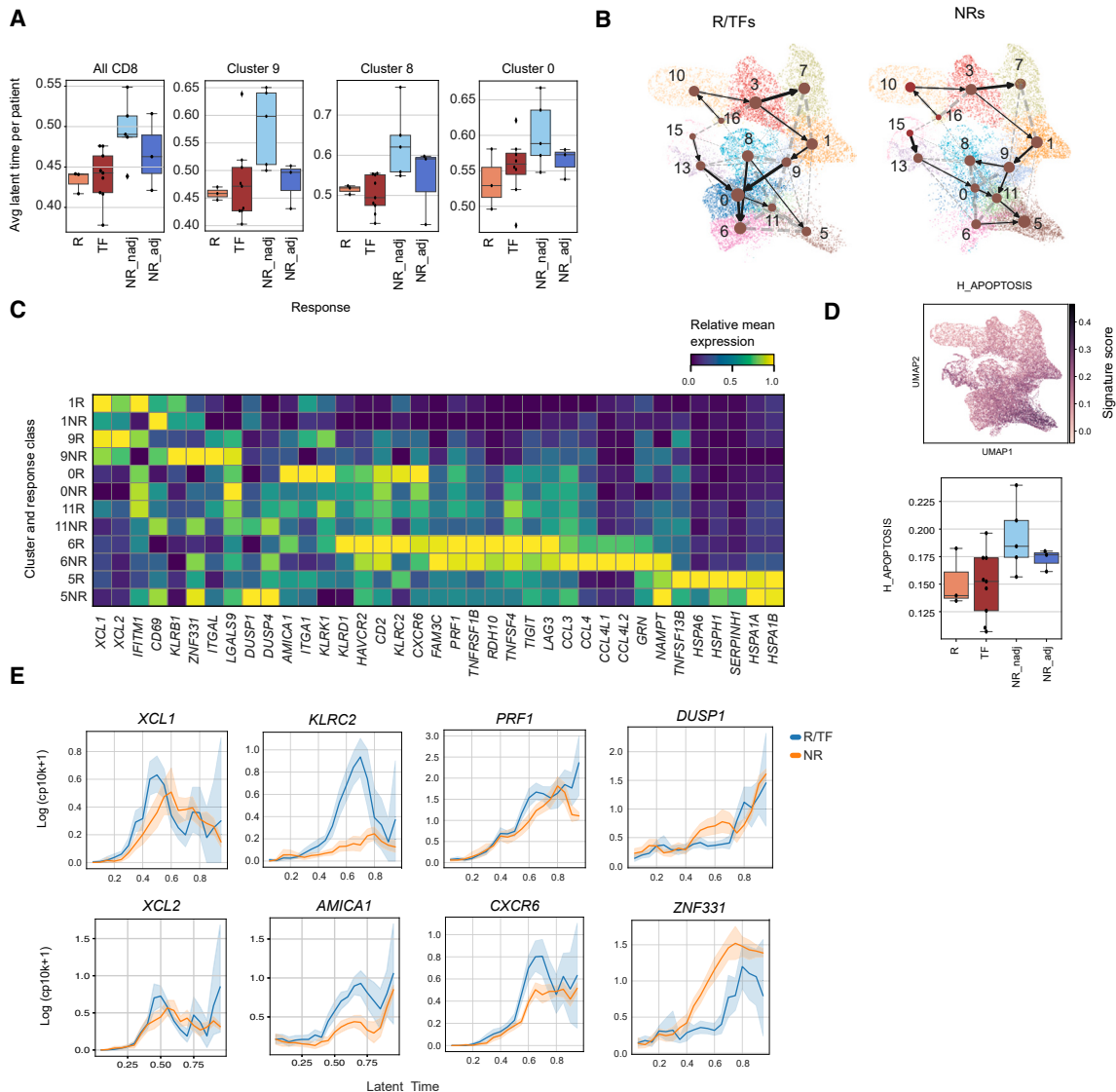
Figure 6. NR CD8+ T cells are characterized by increased cellular stress and hypoxia

(A) Latent time summarized per patient and response class across all analyzed CD8+ T cells (left) or selected clusters (Adj and Nadj).

(B) PAGA-estimated transitions between CD8+ T cell clusters, stratified by response.

(C) Relative (standardized column-wise) mean expression of velocity driver genes (stratified per response class) that are also significantly differentially expressed between R and NR; expression is summarized per cluster of interest and response class.

(D) Hallmark apoptosis signature score across all CD8+ T cells (top), summarized per sample and response class (bottom).

(E) Expression of selected genes (from C) across groups of CD8+ T cells, ordered according to increasing latent time values and stratified by response.

analysis revealed genes associated with T cell effector function and activation, including *IFNG*, *GZMB*, and *GZMH* (Figures 6C and S6G; Table S6),[67–71] among the most highly ranked in Rs/TFs. Meanwhile, cell-state transitions in NRs were driven by genes associated with inhibition of T cell functionality (*DUSP1* and *TSC22D3*), cellular stress (*HSPA1A/1B*, *PPP1R15A*, and *DNAJA1*), and T cell quiescence and exhaustion (*BTG1*)[72–77] (Figures 6C and S6G; Table S6). Comparing the terminal clusters 5 (NRs) to 6 (Rs/TFs), we identified genes similar to those found in the velocity analysis; cells of cluster 6 preferentially expressed *PRF1*, *TNFRSF1B*, *TIGIT*, *CCL4L1/2*, *KLRD1*, and *CXCR6* (among others, including *KLRC2*), while cluster 5 showed high expression of *HSPA1A/1B/A6*, *ATF3*, *SERPINH1*, *DUSP1*, and

DNAJA1 (among others, including *PMAIP1*) as well as a general enrichment of apoptosis and hypoxia pathways (Figures 6C, 6D, and S6G–S6I; Tables S4 and S5), consistent with the results of the overall CD8$^+$ R vs. NR comparison (Figure 3E).

When examining gene expression along the latent time axis for selected genes, we observed that, early on, CD8$^+$ T cells of R/TF patients expressed higher levels of *XCL1*, a gene known to interact through XCR1 with cDC1s,[78] further supporting the notion that the XCR1-XCL1 axis may be more active in R/TF patients (Figures 3 and 6E). R-specific up-regulation along the time axis was also observed for *CXCR6*, *KLRC2*, *AMICA1*, and *PRF1*, markers of antigen-experienced and cytotoxic T cells[79] (Figure 6E). In NRs, we observed a transient early increase of *DUSP1*, involved in inhibition of Th1 polarization, T cell activation, and regulation of regulatory T cell survival. We note that we also detected differences in genes of still unknown function in effector T cells, such as the transcription factor ZNF331, consistently upregulated in NR patients, similar to what we observed previously in the myeloid compartment (Figure 2).

In conclusion, we found the trajectory of CD8$^+$ T cells in R/TF patients to lead toward a population of cells that, alongside classical exhaustion markers, preferentially expressed genes involved in T cell maintenance and effector function, consistent with the notion that, in these patients, pro-inflammatory myeloid-T cell interactions are supporting a sustained anti-tumor response that could be enhanced by CIT. In contrast, in NR patients, the path progresses into a population showing high expression of genes associated with suppressive effects on T cell functionality, cellular stress, and hypoxia.

DISCUSSION

Despite notable progress in the treatment of metastatic melanoma brought about by CITs[1,2,10] and a highly improved biological understanding of disease characteristics at the molecular level,[80] a substantial proportion of patients exhibit an insufficiently explained lack of response. While several studies have attempted to address this gap by providing increased molecular resolution of the tumor microenvironment[14–17,20,81] and related various identified features to response patterns, few stable biomarkers beyond TMB and IFNG/T effector-related gene expression have emerged.[25] In addition, no study has systematically explored the relationship between paired blood and tumor immune cell populations in great depth, despite the fact that often, in the clinical setting, only peripheral blood samples are available. Our study uniquely explores and connects the immune cell diversity in tumors to that in the blood, focusing on the interplay between myeloid and T cell subsets and their link to CPI response. Our analyses confirm previously observed associations between immune cell compartments and response, and we generate novel evidence that can be subsequently followed up in larger cohorts and/or with functional experiments.

Our study reveals that there are marked differences in both cell subtypes and their frequencies between tumors and peripheral blood. Closely inspecting tumor-derived immune cell populations, we showed that the relative composition differs in relation to lesion origin and/or mutational (BRAF vs. NRAS) status. While the association of mutational status and lesion cannot be disentangled given the current cohort size, higher B/naive T cell fractions in lymph node lesions meet the general expectation. In addition, the myeloid phenotype of brain lesions could partially be explained by the presence of microglia. Together, our findings strongly suggest

Med
Article

CellPress

that both immune cell origin and patient mutation status should be recorded and considered in future investigations.

In line with observations of other studies,[26] we found higher levels of classical monocytes in the peripheral blood of R/TF patients prior to CPI treatment. Analyzing matched PBMCs and tumor immune cells, we observed a correlation of classical monocytes' relative fraction in blood to that of classical monocytes and macrophages in tumor lesions. Further, by performing velocity analysis, we captured the transition of classical monocytes into macrophages upon tissue entry, similar to previous studies focusing on other indications.[82] Strikingly, the transitional cell population expressed genes involved in modulating cell (or specifically monocyte/macrophage) migration[34,37,83–85] and inflammatory response,[32] such as *MARCKSL1*, *CD36*, *SELL*, and *S100A8/9/12*, among others. In R/TF patients, the transitional monocytes followed a differentiation path leading to *CXCL9/10*-expressing macrophages, also characterized by high levels of interferon (IFN)-induced genes, such as *IFIT2/3* and *ISG15*. *CXCL9* and *CXCL10* are IFN-gamma pathway members and have been reported previously to induce Th1 polarization.[86] *CXCL9* has also been consistently positively associated with CIT response.[25] In addition, type I IFN production by intratumoral myeloids has been shown to induce NK cell-DC crosstalk, associated with improved response to CPI treatment.[48] Further, the activation of R/TF macrophage-enriched *TREM1* has been found recently to stimulate anti-tumor immunity.[87] Thus, prior to CPI treatment, the tumor immune interactions of R/TF patients support M1-like macrophage differentiation and putative recruitment of cytotoxic T and NK cells.

In contrast, in NR patients, we found transitional monocytes to preferentially differentiate into a monocyte-like cell population, showing relatively low MHC gene expression but high *IL10*, *NLRP3*, *PTX3*, *IL1B*, and *CXCL2* levels, reminiscent of so-called "myeloid-derived suppressor cells" (MDSCs).[88,89] While the immunosuppressive and tolerogenic functions of *IL10* are broadly known,[90] *PTX3* has been reported previously to be involved in inhibiting macrophage activation and HLA-DR expression.[91] Further, tumor-associated NLRP3/IL-1 signaling has been suggested to induce expansion of MDSCs and reduced NK/CD8^{+} T cell activity, while NLRP3 inhibition reduced melanoma progression.[92] Consistently, we also found NR patients to preferentially display predicted myeloid-T/NK cell interactions that were indicative of immunosuppression and apoptosis, most notably those involving TNF, shown previously to dampen CD8^{+} T cell antitumor reactivity.[51]

The presence of cDC1 has been associated with better clinical outcome in cancer patients.[93–95] In line with that, we found a higher frequency of cross-presenting cDC1s, enriched *XCR1-XCL1/2* predicted interactions between cDC1 and T/NK cells, as well as higher levels of *XCL1/2* in T and NK cells in tumors of R/TF patients. Activated CD56-bright NK cells have been described as a main source of *XCL1* expression, consistent with their predominance among the NK populations we describe here.[96] NK cells have been described to pave the way for recruitment of cDC1 into the tumor microenvironment, promoting cancer immune control.[48,93] These findings further support the notion that R and TF tumors present a microenvironment that promotes cross-priming and activation of tumor-directed T cells, whereas the environment of NR tumors shapes differentiation into terminal exhaustion and cellular stress.

Consistently, the analysis of the CD4^{+} T cell compartment revealed that, in NR patients, cell differentiation and cellular interactions were mainly driven by genes associated with cellular stress and apoptosis. Further, the CD8^{+} T cell analysis found

CD8$^+$ T cells in R/TFs to be less advanced in their path toward terminal differentiation, in line with previous studies associating naive/memory CD8$^+$ T cell subsets with better response.[15] In contrast, in the tumors of NR patients, CD8$^+$ T cells showed a differentiation trajectory leading to a state of terminal exhaustion associated with an enrichment of genes related to reduced effector function, apoptosis, cellular stress, and hypoxia. *TSC22D3*, *BTG1*, and *HSPA1A/B* were among the top genes driving the differentiation of CD8$^+$ T cells in NR patients. *TSC22D3* has been described to inhibit *NFKB1* nuclear translocation,[97] *BTG1* to support T cell quiescence[76] and, more recently, the induction of exhausted CD8$^+$ T cells.[77] These findings are suggestive of an improper activation of CD8$^+$ T cells, which may lack the stimuli that support T cell maintenance and function[67,73] in the tumors of NR patients. Interestingly, hypoxia has been shown recently to lead to expansion of more terminally exhausted CD8$^+$ T cells *in vitro*[98] and has been proposed as a putative explanation for the negative association between CD8$^+$ T cell infiltration and CIT response observed in renal cell carcinoma[99,100] as well as a mediator of CIT resistance in pancreatic cancer.[101] Our results raise the intriguing possibility that hypoxia may also mediate CIT resistance in a subset of melanoma patients by altering the phenotype of CD8$^+$ T effector cells. Finally, our findings are also in line with a recent report that identified the association between a stress response state of T cells and resistance to CPI treatment across several cancer types.[102]

Conclusions
In conclusion, our study illustrates that the tumor immune microenvironment prior to CPI treatment can be indicative of response. Features enriched in NR patients include the preferential transition of monocytes into immunosuppressive myeloid cells, enrichment of predicted immunosuppressive myeloid-lymphoid cell interactions, and more frequent transition of CD4$^+$ and CD8$^+$ T cells into a terminally exhausted, apoptotic state. In contrast, Rs showed a high frequency of classical monocytes in the peripheral blood; a preferential transition of monocytes into *CXCL9*-expressing, M1-like macrophages upon tumor entry; a high frequency of cDC1s and cDC1-derived XCR1-XCL1 interactions; as well as a CD8$^+$ T cell expression profile suggestive of a productive effector state. Collectively, these findings pose an opportunity to derive novel ways of complementing classical CPI therapy by targeting pathways involved in myeloid-T cell interactions or immune cell state transitions toward supporting an anti-tumorigenic microenvironment and maintaining T cell functionality to ultimately improve responsiveness.

Limitations of the study
Our cohort is limited by low patient numbers and high heterogeneity due to distinct clinical (e.g., treatment types) and biological (e.g., lesion location) factors. While results should be interpreted with caution, the strength of our study lies in the combined analysis of matched peripheral blood and tumor lesions and the identification of transitional cell states linking the two. Functional validation *in vivo* or using patient-derived tumor explants could strengthen our findings regarding the impact of myeloid-T cell interactions and immune cell state transitions on CPI response.

STAR★METHODS
Detailed methods are provided in the online version of this paper and include the following:

- KEY RESOURCES TABLE
- RESOURCE AVAILABILITY
  - Lead contact

Med
Article

CellPress

- ○ Materials availability
- ○ Data and code availability
- ● EXPERIMENTAL MODEL AND STUDY PARTICIPANT DETAILS
  - ○ Patient samples
- ● METHOD DETAILS
  - ○ Tumor dissociation
  - ○ Flow cytometry
  - ○ Tumor mutational burden measurements
  - ○ Single cell RNA-sequencing
- ● QUANTIFICATION AND STATISTICAL ANALYSIS
  - ○ Single cell RNA-sequencing data processing
  - ○ Trajectory and velocity analysis
  - ○ Cell-cell interaction analysis
  - ○ Differential cell abundance
  - ○ Differential expression analysis
  - ○ Pathway enrichment analysis
  - ○ Pseudo-bulk analysis
  - ○ Other scRNA-seq related analyses

SUPPLEMENTAL INFORMATION

Supplemental information can be found online at https://doi.org/10.1016/j.medj.2024.03.015.

AUTHOR CONTRIBUTIONS

R.S., A.I., M.P.L., and M.B. designed the study. A.I., J.M.M.G., R.D., and M.P.L. provided the samples. R.S., T.H., A.I., S.D., M.M., J.M.M.G., A.R., F.L., E.Y., and J.S. performed sample processing. P.C.S., J.S.-P., and T.K.-T. performed data and statistical analyses. P.C.S. and R.S. had unrestricted access to all data. R.S., P.C.S., S.D., S. Herter, S. Hoves, I.G.d.M., P.U., M.B., and M.P.L. performed data interpretation. R.S., P.C.S., and S.D. wrote the manuscript. All authors read and approved the final version of the manuscript, take responsibility for its content, and agreed to submission.

DECLARATION OF INTERESTS

R.S., S. Hoves, M.B., T.H., S.D., E.Y., F.L., S. Herter, P.U., A.I., J.S., J.S.-P., T.K.-T., I.G.d.M., and P.C.S. are employed by and hold F. Hoffmann-La Roche Ltd. company stock. P.U. and M.B. disclose ownership of F. Hoffmann-La Roche Ltd. patents. R.D. has intermittent, project-focused consulting and/or advisory relationships with Novartis, Merck Sharp & Dohme (MSD), Bristol-Myers Squibb (BMS), Roche, Amgen, Takeda, Pierre Fabre, Sun Pharma, Sanofi, Catalym, Second Genome, Regeneron, Alligator, T3 Pharma, MaxiVAX SA, Pfizer, and touchIME outside of the submitted work. M.P.L. receives project-specific research support outside of the scope of this work from Roche, Novartis, Molecular Partners, and Oncobit.

Med
Article

REFERENCES

1. Switzer, B., Puzanov, I., Skitzki, J.J., Hamad, L., and Ernstoff, M.S. (2022). Managing Metastatic Melanoma in 2022: A Clinical Review. Jco Oncol Pract. *18*, 335–351. https://doi.org/10.1200/op.21.00686.

2. Huang, A.C., and Zappasodi, R. (2022). A decade of checkpoint blockade immunotherapy in melanoma: understanding the molecular basis for immune sensitivity and resistance. Nat. Immunol. *23*, 660–670. https://doi.org/10.1038/s41590-022-01141-1.

3. Alexandrov, L.B., Nik-Zainal, S., Wedge, D.C., Aparicio, S.A.J.R., Behjati, S., Biankin, A.V., Bignell, G.R., Bolli, N., Borg, A., Børresen-Dale, A.L., et al. (2013). Signatures of mutational processes in human cancer. Nature *500*, 415–421. https://doi.org/10.1038/nature12477.

4. Rosenberg, S.A., Yang, J.C., Sherry, R.M., Kammula, U.S., Hughes, M.S., Phan, G.Q., Citrin, D.E., Restifo, N.P., Robbins, P.F., Wunderlich, J.R., et al. (2011). Durable Complete Responses in Heavily Pretreated Patients with Metastatic Melanoma Using T-Cell Transfer Immunotherapy. Clin. Cancer Res. *17*, 4550–4557. https://doi.org/10.1158/1078-0432.ccr-11-0116.

5. Hodi, F.S., O'Day, S.J., McDermott, D.F., Weber, R.W., Sosman, J.A., Haanen, J.B., Gonzalez, R., Robert, C., Schadendorf, D., Hassel, J.C., et al. (2010). Improved Survival with Ipilimumab in Patients with Metastatic Melanoma. New Engl J Medicine *363*, 711–723. https://doi.org/10.1056/nejmoa1003466.

6. Robert, C., Thomas, L., Bondarenko, I., O'Day, S., Weber, J., Garbe, C., Lebbe, C., Baurain, J.-F., Testori, A., Grob, J.-J., et al. (2011). Ipilimumab plus Dacarbazine for Previously Untreated Metastatic Melanoma. New Engl J Medicine *364*, 2517–2526. https://doi.org/10.1056/nejmoa1104621.

7. Robert, C., Long, G.V., Brady, B., Dutriaux, C., Maio, M., Mortier, L., Hassel, J.C., Rutkowski, P., McNeil, C., Kalinka-Warzocha, E., et al. (2015). Nivolumab in Previously Untreated Melanoma without BRAF Mutation. New Engl J Medicine *372*, 320–330. https://doi.org/10.1056/nejmoa1412082.

8. Robert, C., Ribas, A., Schachter, J., Arance, A., Grob, J.-J., Mortier, L., Daud, A., Carlino, M.S., McNeil, C.M., Lotem, M., et al. (2019). Pembrolizumab versus ipilimumab in advanced melanoma (KEYNOTE-006): post-hoc 5-year results from an open-label, multicentre, randomised, controlled, phase 3 study. Lancet Oncol. *20*, 1239–1251. https://doi.org/10.1016/s1470-2045(19)30388-2.

9. Ascierto, P.A., Long, G.V., Robert, C., Brady, B., Dutriaux, C., Di Giacomo, A.M., Mortier, L., Hassel, J.C., Rutkowski, P., McNeil, C., et al. (2019). Survival Outcomes in Patients With Previously Untreated BRAF Wild-Type Advanced Melanoma Treated With Nivolumab Therapy. JAMA Oncol. *5*, 187–194. https://doi.org/10.1001/jamaoncol.2018.4514.

10. Curti, B.D., and Faries, M.B. (2021). Recent Advances in the Treatment of Melanoma. New Engl. J. Med. *384*, 2229–2240. https://doi.org/10.1056/nejmra2034861.

11. Wolchok, J.D., Chiarion-Sileni, V., Gonzalez, R., Grob, J.-J., Rutkowski, P., Lao, C.D., Cowey, C.L., Schadendorf, D., Wagstaff, J., Dummer, R., et al. (2022). Long-Term Outcomes With Nivolumab Plus Ipilimumab or Nivolumab Alone Versus Ipilimumab in Patients With Advanced Melanoma. J. Clin. Oncol. *40*, 127–137. https://doi.org/10.1200/jco.21.02229.

12. Larkin, J., Chiarion-Sileni, V., Gonzalez, R., Grob, J.-J., Rutkowski, P., Lao, C.D., Cowey, C.L., Schadendorf, D., Wagstaff, J., Dummer, R., et al. (2019). Five-Year Survival with Combined Nivolumab and Ipilimumab in Advanced Melanoma. New Engl. J Med. *381*, 1535–1546. https://doi.org/10.1056/nejmoa1910836.

13. Tawbi, H.A., Schadendorf, D., Lipson, E.J., Ascierto, P.A., Matamala, L., Gutiérrez, E.C., Rutkowski, P., Gogas, H.J., Lao, C.D., Menezes, J.J.D., et al. (2022). Relatlimab and Nivolumab versus Nivolumab in Untreated Advanced Melanoma. New Engl. J Med. *386*, 24–34. https://doi.org/10.1056/nejmoa2109970.

14. Tirosh, I., Izar, B., Prakadan, S.M., Wadsworth, M.H., 2nd, Treacy, D., Trombetta, J.J., Rotem, A., Rodman, C., Lian, C., Murphy, G., et al. (2016). Dissecting the multicellular ecosystem of metastatic melanoma by single-cell RNA-seq. Science *352*, 189–196. https://doi.org/10.1126/science.aad0501.

15. Sade-Feldman, M., Yizhak, K., Bjorgaard, S.L., Ray, J.P., de Boer, C.G., Jenkins, R.W., Lieb, D.J., Chen, J.H., Frederick, D.T., Barzily-Rokni, M., et al. (2018). Defining T Cell States Associated with Response to Checkpoint Immunotherapy in Melanoma. Cell *175*, 998–1013.e20. https://doi.org/10.1016/j.cell.2018.10.038.

16. Jerby-Arnon, L., Shah, P., Cuoco, M.S., Rodman, C., Su, M.-J., Melms, J.C., Leeson, R., Kanodia, A., Mei, S., Lin, J.-R., et al. (2018). A Cancer Cell Program Promotes T Cell Exclusion and Resistance to Checkpoint Blockade. Cell *175*, 984–997.e24. https://doi.org/10.1016/j.cell.2018.09.006.

17. Li, H., van der Leun, A.M., Yofe, I., Lubling, Y., Gelbard-Solodkin, D., van Akkooi, A.C.J., van den Braber, M., Rozeman, E.A., Haanen, J.B.A.G., Blank, C.U., et al. (2019). Dysfunctional CD8 T Cells Form a Proliferative, Dynamically Regulated Compartment within Human Melanoma. Cell *176*, 775–789.e18. https://doi.org/10.1016/j.cell.2018.11.043.

18. Oliveira, G., Stromhaug, K., Cieri, N., Iorgulescu, J.B., Klaeger, S., Wolff, J.O., Rachimi, S., Chea, V., Krause, K., Freeman, S.S., et al. (2022). Landscape of helper and regulatory antitumour CD4+ T cells in melanoma. Nature *605*, 532–538. https://doi.org/10.1038/s41586-022-04682-5.

19. Nieto, P., Elosua-Bayes, M., Trincado, J.L., Marchese, D., Massoni-Badosa, R., Salvany, M., Henriques, A., Nieto, J., Aguilar-Fernández, S., Mereu, E., et al. (2021). A single-cell tumor immune atlas for precision oncology. Genome Res. *31*, 1913–1926. https://doi.org/10.1101/gr.273300.120.

20. Irmisch, A., Bonilla, X., Chevrier, S., Lehmann, K.-V., Singer, F., Toussaint, N.C., Esposito, C., Mena, J., Milani, E.S., Casanova, R., et al. (2021). The Tumor Profiler Study: integrated, multi-omic, functional tumor profiling for clinical decision support. Cancer Cell *39*, 288–293. https://doi.org/10.1016/j.ccell.2021.01.004.

21. Im, S.J., Hashimoto, M., Gerner, M.Y., Lee, J., Kissick, H.T., Burger, M.C., Shan, Q., Hale, J.S., Lee, J., Nasti, T.H., et al. (2016). Defining CD8+ T cells that provide the proliferative burst after PD-1 therapy. Nature *537*, 417–421. https://doi.org/10.1038/nature19330.

22. Miller, B.C., Sen, D.R., Al Abosy, R., Bi, K., Virkud, Y.V., LaFleur, M.W., Yates, K.B., Lako, A., Felt, K., Naik, G.S., et al. (2019). Subsets of exhausted CD8+ T cells differentially mediate tumor control and respond to checkpoint blockade. Nat. Immunol. *20*, 326–336. https://doi.org/10.1038/s41590-019-0312-6.

23. Siddiqui, I., Schaeuble, K., Chennupati, V., Fuertes Marraco, S.A., Calderon-Copete, S., Pais Ferreira, D., Carmona, S.J., Scarpellino, L., Gfeller, D., Pradervand, S., et al. (2019). Intratumoral Tcf1+PD-1+CD8+ T Cells with Stem-like Properties Promote Tumor Control in Response to Vaccination and Checkpoint Blockade Immunotherapy. Immunity *50*, 195–211.e10. https://doi.org/10.1016/j.immuni.2018.12.021.

24. Jadhav, R.R., Im, S.J., Hu, B., Hashimoto, M., Li, P., Lin, J.-X., Leonard, W.J., Greenleaf, W.J., Ahmed, R., and Goronzy, J.J. (2019). Epigenetic signature of PD-1+ TCF1+ CD8 T cells that act as resource cells during chronic viral infection and respond to PD-1 blockade. Proc National Acad Sci *116*, 14113–14118. https://doi.org/10.1073/pnas.1903520116.

25. Litchfield, K., Reading, J.L., Puttick, C., Abbosh, C., Bentham, R., Watkins, T.B.K., Rosenthal, R., Biswas, D., Lim, E., AL-Bakir, M., et al. (2020). Meta-analysis of Tumor and T Cell Intrinsic Mechanisms of Sensitization to Checkpoint Inhibition. https://doi.org/10.21203/rs.3.rs-76468/v1.

26. Krieg, C., Nowicka, M., Guglietta, S., Schindler, S., Hartmann, F.J., Weber, L.M., Dummer, R., Robinson, M.D., Levesque, M.P., and Becher, B. (2018). High-dimensional single-cell analysis predicts response to anti-PD-1 immunotherapy. Nat. Med. *24*, 144–153. https://doi.org/10.1038/nm.4466.

27. Lange, M., Bergen, V., Klein, M., Setty, M., Reuter, B., Bakhti, M., Lickert, H., Ansari, M., Schniering, J., Schiller, H.B., et al. (2022). CellRank for directed single-cell fate mapping. Nat. Methods *19*, 159–170. https://doi.org/10.1038/s41592-021-01346-6.

28. Wolf, F.A., Hamey, F.K., Plass, M., Solana, J., Dahlin, J.S., Göttgens, B., Rajewsky, N., Simon, L., and Theis, F.J. (2019). PAGA: graph abstraction reconciles clustering with trajectory inference through a topology preserving map of single cells. Genome Biol. *20*, 59. https://doi.org/10.1186/s13059-019-1663-x.

Med
Article

🔷 CellPress

29. La Manno, G., Soldatov, R., Zeisel, A., Braun, E., Hochgerner, H., Petukhov, V., Lidschreiber, K., Kastriti, M.E., Lönnerberg, P., Furlan, A., et al. (2018). RNA velocity of single cells. Nature 560, 494–498. https://doi.org/10.1038/s41586-018-0414-6.

30. Bergen, V., Lange, M., Peidli, S., Wolf, F.A., and Theis, F.J. (2020). Generalizing RNA velocity to transient cell states through dynamical modeling. Nat. Biotechnol. 38, 1408–1414. https://doi.org/10.1038/s41587-020-0591-3.

31. Auffray, C., Fogg, D., Garfa, M., Elain, G., Join-Lambert, O., Kayal, S., Sarnacki, S., Cumano, A., Lauvau, G., and Geissmann, F. (2007). Monitoring of Blood Vessels and Tissues by a Population of Monocytes with Patrolling Behavior. Science 317, 666–670. https://doi.org/10.1126/science.1142883.

32. Wang, S., Song, R., Wang, Z., Jing, Z., Wang, S., and Ma, J. (2018). S100A8/A9 in Inflammation. Front. Immunol. 9, 1298. https://doi.org/10.3389/fimmu.2018.01298.

33. Foell, D., Wittkowski, H., Vogl, T., and Roth, J. (2007). S100 proteins expressed in phagocytes: a novel group of damage-associated molecular pattern molecules. J. Leukocyte Biol. 81, 28–37. https://doi.org/10.1189/jlb.0306170.

34. Park, Y.M., Febbraio, M., and Silverstein, R.L. (2009). CD36 modulates migration of mouse and human macrophages in response to oxidized LDL and may contribute to macrophage trapping in the arterial intima. J. Clin. Invest. 119, 136–145. https://doi.org/10.1172/jci35535.

35. El Amri, M., Fitzgerald, U., and Schlosser, G. (2018). MARCKS and MARCKS-like proteins in development and regeneration. JJ. Biomed. Sci. 25, 43. https://doi.org/10.1186/s12929-018-0445-1.

36. Li, J., and Aderem, A. (1992). MacMARCKS, a novel member of the MARCKS family of protein kinase C substrates. Cell 70, 791–801. https://doi.org/10.1016/0092-8674(92)90312-z.

37. Chun, K.-R., Bae, E.M., Kim, J.-K., Suk, K., and Lee, W.-H. (2009). Suppression of the lipopolysaccharide-induced expression of MARCKS-related protein (MRP) affects transmigration in activated RAW264.7 cells. Cell. Immunol. 256, 92–98. https://doi.org/10.1016/j.cellimm.2009.01.011.

38. Hickey, M.J., Forster, M., Mitchell, D., Kaur, J., De Caigny, C., and Kubes, P. (2000). L-Selectin Facilitates Emigration and Extravascular Locomotion of Leukocytes During Acute Inflammatory Responses In Vivo. JJ. Immunol. 165, 7164–7170. https://doi.org/10.4049/jimmunol.165.12.7164.

39. Tsang, Y.T., Neelamegham, S., Hu, Y., Berg, E.L., Burns, A.R., Smith, C.W., and Simon, S.I. (1997). Synergy between L-selectin signaling and chemotactic activation during neutrophil adhesion and transmigration. J Immunol Baltim Md 1950 159, 4566–4577.

40. Brckalo, T., Calzetti, F., Pérez-Cabezas, B., Borràs, F.E., Cassatella, M.A., and López-Botet, M. (2010). Functional analysis of the CD300e receptor in human monocytes and myeloid dendritic cells. Eur. J. Immunol. 40, 722–732. https://doi.org/10.1002/eji.200939468.

41. Aguilar, H., Álvarez-Errico, D., García-Montero, A.C., Orfao, A., Sayós, J., and López-Botet, M. (2004). Molecular Characterization of a Novel Immune Receptor Restricted to the Monocytic Lineage. JJ. Immunol. 173, 6703–6711. https://doi.org/10.4049/jimmunol.173.11.6703.

42. Clark, G.J., Jamriska, L., Rao, M., and Hart, D.N.J. (2007). Monocytes Immunoselected via the Novel Monocyte Specific Molecule, CD300e, Differentiate Into Active Migratory Dendritic Cells. J. Immunother. 30, 303–311. https://doi.org/10.1097/01.cji.0000211342.65964.9e.

43. Vogel, D.Y.S., Glim, J.E., Stavenuiter, A.W.D., Breur, M., Heijnen, P., Amor, S., Dijkstra, C.D., and Beelen, R.H.J. (2014). Human macrophage polarization in vitro: Maturation and activation methods compared. Immunobiology 219, 695–703. https://doi.org/10.1016/j.imbio.2014.05.002.

44. Cheng, S., Li, Z., Gao, R., Xing, B., Gao, Y., Yang, Y., Qin, S., Zhang, L., Ouyang, H., Du, P., et al. (2021). A pan-cancer single-cell transcriptional atlas of tumor infiltrating myeloid cells. Cell 184, 792–809.e23. https://doi.org/10.1016/j.cell.2021.01.010.

45. Zhang, Q., He, Y., Luo, N., Patel, S.J., Han, Y., Gao, R., Modak, M., Carotta, S., Haslinger, C., Kind, D., et al. (2019). Landscape and Dynamics of Single Immune Cells in Hepatocellular Carcinoma. Cell 179, 829–845.e20. https://doi.org/10.1016/j.cell.2019.10.003.

46. Sharma, A., Seow, J.J.W., Dutertre, C.-A., Pai, R., Blériot, C., Mishra, A., Wong, R.M.M., Singh, G.S.N., Sudhagar, S., Khalilnezhad, S., et al. (2020). Onco-fetal Reprogramming of Endothelial Cells Drives Immunosuppressive Macrophages in Hepatocellular Carcinoma. Cell 183, 377–394.e21. https://doi.org/10.1016/j.cell.2020.08.040.

47. Mulder, K., Patel, A.A., Kong, W.T., Piot, C., Halitzki, E., Dunsmore, G., Khalilnezhad, S., Irac, S.E., Dubuisson, A., Chevrier, M., et al. (2021). Cross-tissue single-cell landscape of human monocytes and macrophages in health and disease. Immunity 54, 1883–1900.e5. https://doi.org/10.1016/j.immuni.2021.07.007.

48. Lam, K.C., Araya, R.E., Huang, A., Chen, Q., Di Modica, M., Rodrigues, R.R., Lopès, A., Johnson, S.B., Schwarz, B., Bohrnsen, E., et al. (2021). Microbiota triggers STING-type I IFN-dependent monocyte reprogramming of the tumor microenvironment. Cell 184, 5338–5356.e21. https://doi.org/10.1016/j.cell.2021.09.019.

49. Efremova, M., Vento-Tormo, M., Teichmann, S.A., and Vento-Tormo, R. (2020). CellPhoneDB: inferring cell–cell communication from combined expression of multi-subunit ligand–receptor complexes. Nat. Protoc. 15, 1484–1506. https://doi.org/10.1038/s41596-020-0292-x.

50. Wang, S., and El-Deiry, W.S. (2003). TRAIL and apoptosis induction by TNF-family death receptors. Oncogene 22, 8628–8633. https://doi.org/10.1038/sj.onc.1207232.

51. Donia, M., Andersen, R., Kjeldsen, J.W., Fagone, P., Munir, S., Nicoletti, F., Andersen, M.H., Thor Straten, P., and Svane, I.M. (2015). Aberrant Expression of MHC Class II in Melanoma Attracts Inflammatory Tumor-Specific CD4+ T- Cells, Which Dampen CD8+ T-cell Antitumor Reactivity. Cancer Res. 75, 3747–3759. https://doi.org/10.1158/0008-5472.can-14-2956.

52. Zhao, X., Rong, L., Zhao, X., Li, X., Liu, X., Deng, J., Wu, H., Xu, X., Erben, U., Wu, P., et al. (2012). TNF signaling drives myeloid-derived suppressor cell accumulation. J. Clin. Invest. 122, 4094–4104. https://doi.org/10.1172/jci64115.

53. Webster, J.D., and Vucic, D. (2020). The Balance of TNF Mediated Pathways Regulates Inflammatory Cell Death Signaling in Healthy and Diseased Tissues. Frontiers Cell Dev Biology 8, 365. https://doi.org/10.3389/fcell.2020.00365.

54. Audrito, V., Serra, S., Brusa, D., Mazzola, F., Arruga, F., Vaisitti, T., Coscia, M., Maffei, R., Rossi, D., Wang, T., et al. (2015). Extracellular nicotinamide phosphoribosyltransferase (NAMPT) promotes M2 macrophage polarization in chronic lymphocytic leukemia. Blood 125, 111–123. https://doi.org/10.1182/blood-2014-07-589069.

55. Yang, L., Froio, R.M., Sciuto, T.E., Dvorak, A.M., Alon, R., and Luscinskas, F.W. (2005). ICAM-1 regulates neutrophil adhesion and transcellular migration of TNF-alpha-activated vascular endothelium under flow. Blood 106, 584–592. https://doi.org/10.1182/blood-2004-12-4942.

56. Blank, C., Brown, I., Kacha, A.K., Markiewicz, M.A., and Gajewski, T.F. (2005). ICAM-1 Contributes to but Is Not Essential for Tumor Antigen Cross-Priming and CD8+ T Cell-Mediated Tumor Rejection In Vivo. JJ. Immunol. 174, 3416–3420. https://doi.org/10.4049/jimmunol.174.6.3416.

57. Leitner, J., Herndler-Brandstetter, D., Zlabinger, G.J., Grubeck-Loebenstein, B., and Steinberger, P. (2015). CD58/CD2 Is the Primary Costimulatory Pathway in Human CD28−CD8+ T Cells. JJ. Immunol. 195, 477–487. https://doi.org/10.4049/jimmunol.1401917.

58. Rölle, A., Halenius, A., Ewen, E.M., Cerwenka, A., Hengel, H., and Momburg, F. (2016). CD2–CD58 interactions are pivotal for the activation and function of adaptive natural killer cells in human cytomegalovirus infection. Eur. J. Immunol. 46, 2420–2425. https://doi.org/10.1002/eji.201646492.

59. Dorner, B.G., Dorner, M.B., Zhou, X., Opitz, C., Mora, A., Güttler, S., Hutloff, A., Mages, H.W., Ranke, K., Schaefer, M., et al. (2009). Selective Expression of the Chemokine Receptor XCR1 on Cross-presenting Dendritic Cells Determines Cooperation with CD8+ T Cells. Immunity 31, 823–833. https://doi.org/10.1016/j.immuni.2009.08.027.

60. Kroczek, R.A., and Henn, V. (2012). The Role of XCR1 and its Ligand XCL1 in Antigen Cross-Presentation by Murine and Human Dendritic Cells. Front. Immunol. 3, 14. https://doi.org/10.3389/fimmu.2012.00014.

61. Bachem, A., Güttler, S., Hartung, E., Ebstein, F., Schaefer, M., Tannert, A., Salama, A., Movassaghi, K., Opitz, C., Mages, H.W., et al. (2010). Superior antigen cross-presentation and XCR1 expression define human CD11c+CD141+ cells as homologues of mouse CD8+ dendritic cells. JJ. Exp. Med. *207*, 1273–1281. https://doi.org/10.1084/jem.20100348.

62. Sanjabi, S., Mosaheb, M.M., and Flavell, R.A. (2009). Opposing effects of TGF-beta and IL-15 cytokines control the number of short-lived effector CD8+ T cells. Immunity *31*, 131–144. https://doi.org/10.1016/j.immuni.2009.04.020.

63. Rodriguez-Barbosa, J.I., Schneider, P., Weigert, A., Lee, K.-M., Kim, T.-J., Perez-Simon, J.-A., and Rio, M.-L. del (2019). HVEM, a cosignaling molecular switch, and its interactions with BTLA, CD160 and LIGHT. Cell. Mol. Immunol. *16*, 679–682. https://doi.org/10.1038/s41423-019-0241-1.

64. McGraw, J.M., Thelen, F., Hampton, E.N., Bruno, N.E., Young, T.S., Havran, W.L., and Witherden, D.A. (2021). JAML promotes CD8 and γδ T cell antitumor immunity and is a novel target for cancer immunotherapy. JJ. Exp. Med. *218*, e20202644. https://doi.org/10.1084/jem.20202644.

65. Chiang, E.Y., de Almeida, P.E., de Almeida Nagata, D.E., Bowles, K.H., Du, X., Chitre, A.S., Banta, K.L., Kwon, Y., McKenzie, B., Mittman, S., et al. (2020). CD96 functions as a co-stimulatory receptor to enhance CD8+ T cell activation and effector responses. Eur. J. Immunol. *50*, 891–902. https://doi.org/10.1002/eji.201948405.

66. DePasquale, E.A.K., Ssozi, D., Ainciburu, M., Good, J., Noel, J., Villanueva, M.A., Couturier, C.P., Shalek, A.K., Aranki, S.F., Mallidi, H.R., et al. (2022). Single-Cell Multiomics Reveals Clonal T-Cell Expansions and Exhaustion in Blastic Plasmacytoid Dendritic Cell Neoplasm. Front. Immunol. *13*, 809414. https://doi.org/10.3389/fimmu.2022.809414.

67. Chen, Y., Zander, R., Khatun, A., Schauder, D.M., and Cui, W. (2018). Transcriptional and Epigenetic Regulation of Effector and Memory CD8 T Cell Differentiation. Front. Immunol. *9*, 2826. https://doi.org/10.3389/fimmu.2018.02826.

68. Conley, J.M., Gallagher, M.P., and Berg, L.J. (2016). T Cells and Gene Regulation: The Switching On and Turning Up of Genes after T Cell Receptor Stimulation in CD8 T Cells. Front. Immunol. *7*, 76. https://doi.org/10.3389/fimmu.2016.00076.

69. van der Leun, A.M., Thommen, D.S., and Schumacher, T.N. (2020). CD8+ T cell states in human cancer: insights from single-cell analysis. Nat. Rev. Cancer *20*, 218–232. https://doi.org/10.1038/s41568-019-0235-4.

70. Kouno, J., Nagai, H., Nagahata, T., Onda, M., Yamaguchi, H., Adachi, K., Takahashi, H., Teramoto, A., and Emi, M. (2004). Up-regulation of CC chemokine, CCL3L1, and receptors, CCR3, CCR5 in human glioblastoma that promotes cell growth. J. Neurooncol. *70*, 301–307. https://doi.org/10.1007/s11060-004-9165-3.

71. Trifilo, M.J., Bergmann, C.C., Kuziel, W.A., and Lane, T.E. (2003). CC Chemokine Ligand 3 (CCL3) Regulates CD8 + -T-Cell Effector Function and Migration following Viral Infection. J. Virol. *77*, 4004–4014. https://doi.org/10.1128/jvi.77.7.4004-4014.2003.

72. Zhang, Y., Reynolds, J.M., Chang, S.H., Martin-Orozco, N., Chung, Y., Nurieva, R.I., and Dong, C. (2009). MKP-1 Is Necessary for T Cell Activation and Function. J. Biol. Chem. *284*, 30815–30824. https://doi.org/10.1074/jbc.m109.052472.

73. Sun, F., Yue, T.-T., Yang, C.-L., Wang, F.-X., Luo, J.-H., Rong, S.-J., Zhang, M., Guo, Y., Xiong, F., and Wang, C.-Y. (2021). The MAPK dual specific phosphatase (DUSP) proteins: A versatile wrestler in T cell functionality. Int. Immunopharmacol. *98*, 107906. https://doi.org/10.1016/j.intimp.2021.107906.

74. Yan, M., Hu, J., Yuan, H., Xu, L., Liao, G., Jiang, Z., Zhu, J., Pang, B., Ping, Y., Zhang, Y., et al. (2021). Dynamic regulatory networks of T cell trajectory dissect transcriptional control of T cell state transition. Mol. Ther. Nucleic Acids *26*, 1115–1129. https://doi.org/10.1016/j.omtn.2021.10.011.

75. Guan, Y., Zhu, X., Liang, J., Wei, M., Huang, S., and Pan, X. (2021). Upregulation of HSPA1A/HSPA1B/HSPA7 and Downregulation of HSPA9 Were Related to Poor Survival in Colon Cancer. Frontiers Oncol. *11*, 749673. https://doi.org/10.3389/fonc.2021.749673.

76. Hwang, S.S., Lim, J., Yu, Z., Kong, P., Sefik, E., Xu, H., Harman, C.C.D., Kim, L.K., Lee, G.R., Li, H.-B., and Flavell, R.A. (2020). mRNA destabilization by BTG1 and BTG2 maintains T cell quiescence. Science *367*, 1255–1260. https://doi.org/10.1126/science.aax0194.

77. Giles, J.R., Ngiow, S.F., Manne, S., Baxter, A.E., Khan, O., Wang, P., Staupe, R., Abdel-Hakeem, M.S., Huang, H., Mathew, D., et al. (2022). Longitudinal single cell transcriptional and epigenetic mapping of effector, memory, and exhausted CD8 T cells reveals shared biological circuits across distinct cell fates. Preprint at bioRxiv *2022*. 03.27.485974. https://doi.org/10.1101/2022.03.27.485974.

78. Bödder, J., Zahan, T., Slooten, R. van, Schreibelt, G., Vries, I.J.M. de, and Flórez-Grau, G. (2021). Harnessing the cDC1-NK Cross-Talk in the Tumor Microenvironment to Battle Cancer. Front. Immunol. *11*, 631713. https://doi.org/10.3389/fimmu.2020.631713.

79. Melaiu, O., Chierici, M., Lucarini, V., Jurman, G., Conti, L.A., De Vito, R., Boldrini, R., Cifaldi, L., Castellano, A., Furlanello, C., et al. (2020). Cellular and gene signatures of tumor-infiltrating dendritic cells and natural-killer cells predict prognosis of neuroblastoma. Nat. Commun. *11*, 5992. https://doi.org/10.1038/s41467-020-19781-y.

80. Network, T.C.G.A., Akbani, R., Akdemir, K.C., Aksoy, B.A., Albert, M., Ally, A., Amin, S.B., Arachchi, H., Arora, A., Auman, J.T., et al. (2015). Genomic Classification of Cutaneous Melanoma. Cell *161*, 1681–1696. https://doi.org/10.1016/j.cell.2015.05.044.

81. Harel, M., Ortenberg, R., Varanasi, S.K., Mangalhara, K.C., Mardamshina, M., Markovits, E., Baruch, E.N., Tripple, V., Arama-Chayoth, M., Greenberg, E., et al.

(2019). Proteomics of Melanoma Response to Immunotherapy Reveals Mitochondrial Dependence. Cell *179*, 236–250.e18. https://doi.org/10.1016/j.cell.2019.08.012.

82. Zhang, L., Li, Z., Skrzypczynska, K.M., Fang, Q., Zhang, W., O'Brien, S.A., He, Y., Wang, L., Zhang, Q., Kim, A., et al. (2020). Single-Cell Analyses Inform Mechanisms of Myeloid-Targeted Therapies in Colon Cancer. Cell *181*, 442–459.e29. https://doi.org/10.1016/j.cell.2020.03.048.

83. Björklom, B., Padzik, A., Mohammad, H., Westerlund, N., Komulainen, E., Hollos, P., Parviainen, L., Papageorgiou, A.C., Iljin, K., Kallioniemi, O., et al. (2012). c-Jun N-Terminal Kinase Phosphorylation of MARCKSL1 Determines Actin Stability and Migration in Neurons and in Cancer Cells. Mol. Cell. Biol. *32*, 3513–3526. https://doi.org/10.1128/mcb.00713-12.

84. Geissmann, F., Jung, S., and Littman, D.R. (2003). Blood Monocytes Consist of Two Principal Subsets with Distinct Migratory Properties. Immunity *19*, 71–82. https://doi.org/10.1016/s1074-7613(03)00174-2.

85. Xu, H., Manivannan, A., Crane, I., Dawson, R., and Liversidge, J. (2008). Critical but divergent roles for CD62L and CD44 in directing blood monocyte trafficking in vivo during inflammation. Blood *112*, 1166–1174. https://doi.org/10.1182/blood-2007-06-098327.

86. Tokunaga, R., Zhang, W., Naseem, M., Puccini, A., Berger, M.D., Soni, S., McSkane, M., Baba, H., and Lenz, H.-J. (2018). CXCL9, CXCL10, CXCL11/CXCR3 axis for immune activation – A target for novel cancer therapy. Cancer Treat. Rev. *63*, 40–47. https://doi.org/10.1016/j.ctrv.2017.11.007.

87. Juric, V., Mayes, E., Binnewies, M., Lee, T., Canaday, P., Pollack, J.L., Rudolph, J., Du, X., Liu, V.M., Dash, S., et al. (2023). TREM1 activation of myeloid cells promotes antitumor immunity. Sci. Transl. Med. *15*, eadd9990. https://doi.org/10.1126/scitranslmed.add9990.

88. Veglia, F., Sanseviero, E., and Gabrilovich, D.I. (2021). Myeloid-derived suppressor cells in the era of increasing myeloid cell diversity. Nat. Rev. Immunol. *21*, 485–498. https://doi.org/10.1038/s41577-020-00490-y.

89. Wang, Y., Ding, Y., Guo, N., and Wang, S. (2019). MDSCs: Key Criminals of Tumor Pre-metastatic Niche Formation. Front. Immunol. *10*, 172. https://doi.org/10.3389/fimmu.2019.00172.

90. Saraiva, M., Vieira, P., and O'Garra, A. (2020). Biology and therapeutic potential of interleukin-10. JJ. Exp. Med. *217*, e20190418. https://doi.org/10.1084/jem.20190418.

91. Shiraki, A., Kotooka, N., Komoda, H., Hirase, T., Oyama, J., and Node, K. (2016). Pentraxin-3 regulates the inflammatory activity of macrophages. Biochem Biophysics Reports *5*, 290–295. https://doi.org/10.1016/j.bbrep.2016.01.009.

92. Tengesdal, I.W., Menon, D.R., Osborne, D.G., Neff, C.P., Powers, N.E., Gamboni, F., Mauro, A.G., D'Alessandro, A., Stefanoni, D., Henen, M.A., et al. (2021). Targeting tumor-derived NLRP3 reduces melanoma progression by

CellPress

limiting MDSCs expansion. Proc National Acad Sci 118. e2000915118. https://doi.org/10.1073/pnas.2000915118.

93. Böttcher, J.P., Bonavita, E., Chakravarty, P., Blees, H., Cabeza-Cabrerizo, M., Sammicheli, S., Rogers, N.C., Sahai, E., Zelenay, S., and Reis e Sousa, C. (2018). NK Cells Stimulate Recruitment of cDC1 into the Tumor Microenvironment Promoting Cancer Immune Control. Cell 172, 1022–1037.e14. https://doi.org/10.1016/j.cell.2018.01.004.

94. Barry, K.C., Hsu, J., Broz, M.L., Cueto, F.J., Binnewies, M., Combes, A.J., Nelson, A.E., Loo, K., Kumar, R., Rosenblum, M.D., et al. (2018). A natural killer–dendritic cell axis defines checkpoint therapy–responsive tumor microenvironments. Nat. Med. 24, 1178–1191. https://doi.org/10.1038/s41591-018-0085-8.

95. Hubert, M., Gobbini, E., Couillault, C., Manh, T.-P.V., Doffin, A.-C., Berthet, J., Rodriguez, C., Ollion, V., Kielbassa, J., Sajous, C., et al. (2020). IFN-III is selectively produced by cDC1 and predicts good clinical outcome in breast cancer. Sci. Immunol. 5. https://doi.org/10.1126/sciimmunol.aav3942.

96. Yang, C., Siebert, J.R., Burns, R., Gerbec, Z.J., Bonacci, B., Rymaszewski, A., Rau, M., Riese, M.J., Rao, S., Carlson, K.-S., et al. (2019). Heterogeneity of human bone marrow and blood natural killer cells defined by single-cell transcriptome. Nat. Commun. 10, 3931. https://doi.org/10.1038/s41467-019-11947-7.

97. Ayroldi, E., Migliorati, G., Bruscoli, S., Marchetti, C., Zollo, O., Cannarile, L., D'Adamio, F., and Riccardi, C. (2001). Modulation of T-cell activation by the glucocorticoid-induced leucine zipper factor via inhibition of nuclear factor κB. Blood 98, 743–753. https://doi.org/10.1182/blood.v98.3.743.

98. Bannoud, N., Dalotto-Moreno, T., Kindgard, L., García, P.A., Blidner, A.G., Mariño, K.V., Rabinovich, G.A., and Croci, D.O. (2021). Hypoxia Supports Differentiation of Terminally Exhausted CD8 T Cells. Front. Immunol. 12, 660944. https://doi.org/10.3389/fimmu.2021.660944.

99. Giraldo, N.A., Becht, E., Pagès, F., Skliris, G., Verkarre, V., Vano, Y., Mejean, A., Saint-Aubert, N., Lacroix, L., Natario, I., et al. (2015). Orchestration and Prognostic Significance of Immune Checkpoints in the Microenvironment of Primary and Metastatic Renal Cell Cancer. Clin. Cancer Res. 21, 3031–3040. https://doi.org/10.1158/1078-0432.ccr-14-2926.

100. Siska, P.J., Beckermann, K.E., Mason, F.M., Andrejeva, G., Greenplate, A.R., Sendor, A.B., Chiang, Y.-C.J., Corona, A.L., Gemta, L.F., Vincent, B.G., et al. (2017). Mitochondrial dysregulation and glycolytic insufficiency functionally impair CD8 T cells infiltrating human renal cell carcinoma. Jci Insight 2, e93411. https://doi.org/10.1172/jci.insight.93411.

101. Daniel, S.K., Sullivan, K.M., Labadie, K.P., and Pillarisetty, V.G. (2019). Hypoxia as a barrier to immunotherapy in pancreatic adenocarcinoma. Clin Transl Medicine 8, 10. https://doi.org/10.1186/s40169-019-0226-9.

102. Chu, Y., Dai, E., Li, Y., Han, G., Pei, G., Ingram, D.R., Thakkar, K., Qin, J.-J., Dang, M., Le, X., et al. (2023). Pan-cancer T cell atlas links a cellular stress response state to immunotherapy resistance. Nat. Med. 29, 1550–1562. https://doi.org/10.1038/s41591-023-02371-y.

103. Mädler, S.C., Julien-Laferriere, A., Wyss, L., Phan, M., Sonrel, A., Kang, A.S.W., Ulrich, E., Schmucki, R., Zhang, J.D., Ebeling, M., et al. (2021). Besca, a single-cell transcriptomics analysis toolkit to accelerate translational research. NAR Genom. Bioinform 3, lqab102. https://doi.org/10.1093/nargab/lqab102.

104. Wolf, F.A., Angerer, P., and Theis, F.J. (2018). SCANPY: large-scale single-cell gene expression data analysis. Genome Biol. 19, 15. https://doi.org/10.1186/s13059-017-1382-0.

105. Polański, K., Young, M.D., Miao, Z., Meyer, K.B., Teichmann, S.A., and Park, J.-E. (2019). BBKNN: fast batch alignment of single cell transcriptomes. Bioinform Oxf Engl 36, 964–965. https://doi.org/10.1093/bioinformatics/btz625.

106. Fang, Z., Liu, X., and Peltz, G. (2022). GSEApy: a comprehensive package for performing gene set enrichment analysis in Python. Bioinform. (Oxf., Engl.) 39, btac757. https://doi.org/10.1093/bioinformatics/btac757.

107. Robinson, M.D., McCarthy, D.J., and Smyth, G.K. (2010). edgeR: a Bioconductor package for differential expression analysis of digital gene expression data. Bioinformatics 26, 139–140. https://doi.org/10.1093/bioinformatics/btp616.

108. Huber, W., von Heydebreck, A., Sültmann, H., Poustka, A., and Vingron, M. (2002). Variance stabilization applied to microarray data calibration and to the quantification of differential expression. Bioinformatics 18, S96–S104. https://doi.org/10.1093/bioinformatics/18.suppl_1.s96.

109. Wu, D., and Smyth, G.K. (2012). Camera: a competitive gene set test accounting for inter-gene correlation. Nucleic Acids Res. 40, e133. https://doi.org/10.1093/nar/gks461.

110. Bates, D., Mächler, M., Bolker, B., and Walker, S. (2014). Fitting Linear Mixed-Effects Models Using Lme4. Preprint at arXiv. https://doi.org/10.48550/arxiv.1406.5823.

111. Traag, V.A., Waltman, L., and Eck, N.J. van (2019). From Louvain to Leiden: guaranteeing well-connected communities. Sci Rep-uk 9, 5233. https://doi.org/10.1038/s41598-019-41695-z.

112. Diehl, A.D., Meehan, T.F., Bradford, Y.M., Brush, M.H., Dahdul, W.M., Dougall, D.S., He, Y., Osumi-Sutherland, D., Ruttenberg, A., Sarntivijai, S., et al. (2016). The Cell Ontology 2016: enhanced content, modularization, and ontology interoperability. J. Biomed. Semantics 7, 44. https://doi.org/10.1186/s13326-016-0088-7.

113. Wolf, F.A., Hamey, F.K., Plass, M., Solana, J., Dahlin, J.S., Göttgens, B., Rajewsky, N., Simon, L., and Theis, F.J. (2019). PAGA: graph abstraction reconciles clustering with trajectory inference through a topology preserving map of single cells. Genome Biol. 20, 59. https://doi.org/10.1186/s13059-019-1663-x.

114. Nowicka, M., Krieg, C., Crowell, H.L., Weber, L.M., Hartmann, F.J., Guglietta, S., Becher, B., Levesque, M.P., and Robinson, M.D. (2019). CyTOF workflow: differential discovery in high-throughput high-dimensional cytometry datasets. F1000research 6, 748. https://doi.org/10.12688/f1000research.11622.4.

115. Chen, E.Y., Tan, C.M., Kou, Y., Duan, Q., Wang, Z., Meirelles, G.V., Clark, N.R., and Ma'ayan, A. (2013). Enrichr: interactive and collaborative HTML5 gene list enrichment analysis tool. BMC Bioinf. 14, 128. https://doi.org/10.1186/1471-2105-14-128.

116. R-Core-Team (2022). R: A Language and Environment for Statistical Computing (R Foundation for Statistical Computing).

CellPress

Med
Article

STAR★METHODS

KEY RESOURCES TABLE

REAGENT or RESOURCE	SOURCE	IDENTIFIER
Antibodies		
Mouse monoclonal anti-human CD45 FITC	Biolegend	Cat#304006, RRID:AB_314394
Biological samples		
Peripheral blood mononuclear cells of melanoma patients (Table S1)	Department of Dermatology, University Hospital Zurich, Switzerland	N/A
Melanoma tumor specimen (Table S1)	Department of Dermatology, University Hospital Zurich, Switzerland	N/A
Chemicals, peptides, and recombinant proteins		
Accutase	Sigma-Aldrich	Cat#A6964
Collagenase IV	Worthington	Cat#LS004188
DNAse type IV	Sigma-Aldrich	Cat#D5025
Fc block	Biolegend	Cat#422302
Hyaluronidase	Sigma-Aldrich	Cat#H4272
Near-IR APC-Cy7 Live/Dead stain	Thermo Fisher Scientific	Cat#L34976
Critical commercial assays		
Chromium Single Cell 3′ Library & Gel Bead Kit v2, 16 rxns	10x Genomics	Cat#PN-120237
Chromium Single Cell A Chip Kits	10x Genomics	Cat#PN-120236
Chromium i7 Multiplex Kit, 96 rxns	10x Genomics	Cat#PN-120262
SPRIselect Reagent Kit	Beckman-Coulter	Cat#B23318
Qubit dsDNA HS Assay Kit	Thermo Fisher Scientific	Cat#Q32854
High Sensitivity DNA Kit	Agilent	Cat#5067-4626
HiSeq 3000/4000 PE Cluster Kit	Illumina, Inc.	Cat#PE-410-1001
HiSeq 3000/4000 SBS Kit (150 cycles)	Illumina, Inc.	Cat#FC-410-1002
Deposited data		
Single-cell RNA-seq data	ArrayExpress	E-MTAB-13770
Software and algorithms		
cellranger, version 2.1.1	10x Genomics	https://www.10xgenomics.com/support/software/cell-ranger/latest
besca	Mädler et al.[103]	https://github.com/bedapub/besca
scanpy	Wolf et al.[104]	https://scanpy.readthedocs.io/en/stable/index.html
bbknn	Polanski et al.[105]	https://github.com/Teichlab/bbknn
scvelo	Bergen et al.[30]	https://scvelo.readthedocs.io/en/stable/#
cellrank	Lange et al.[27]	https://github.com/theislab/cellrank
velocyto	Manno et al.[29]	https://velocyto.org/velocyto.py/index.html
cellphonedb	Efremova et al.[49]	https://github.com/ventolab/CellPhoneDB
gseapy, enrichr	Fang et al.[106]	https://gseapy.readthedocs.io/en/latest/index.html
edgeR	Robinson et al.[107]	https://bioconductor.org/packages/release/bioc/html/edgeR.html
vsn	Huber et al.[108]	https://bioconductor.org/packages/release/bioc/html/vsn.html
Hmisc	https://hbiostat.org/r/hmisc/	https://cran.r-project.org/web/packages/Hmisc/index.html
camera	Wu et al.[109]	https://rdrr.io/bioc/limma/man/camera.html
lme4	Bates et al.[110]	https://cran.r-project.org/web/packages/lme4/index.html
Code used for data analysis and figure generation	https://zenodo.org/doi/10.5281/zenodo.10792625	https://github.com/bedapub/MelanomaCITResponse_scRNAseq_TILandPBMC_publication
Other		
BD FACS ARIA Fusion III	Becton Dickinson GmbH	https://www.bdbiosciences.com/en-de/products/instruments/flow-cytometers/research-cell-sorters/bd-facsaria-fusion
2100 Bioanalyzer Laptop Bundle	Agilent	Cat#G2943CA
Qubit 3.0 Fluorometer	Thermo Fisher Scientific	Cat#Q33216
Chromium Single Cell Controller	10x Genomics	Cat#PN-120263

(Continued on next page)

Continued		
REAGENT or RESOURCE	SOURCE	IDENTIFIER
Cellometer Auto 2000 Cell Viability Counter	Nexcelom	https://www.nexcelom.com/nexcelom-products/_undercellometer-fluorescent-viability-cell-counters/cellometer-auto-2000/
cBOT	Illumina, Inc.	Cat#SY-301-2002
HiSeq 4000 Sequencer	Illumina, Inc.	Cat#SY-401-4001

RESOURCE AVAILABILITY

Lead contact
Further information and requests for resources and reagents should be directed to and will be fulfilled by the lead contact, Ramona Schlenker (ramona.schlenker@roche.com).

Materials availability
This study did not generate new unique reagents.

Data and code availability
- Single-cell RNA-sequencing data is available in ArrayExpress: E-MTAB-13770 (key resources table).
- Original code related to data analysis and figure generation is shared at https://github.com/bedapub/MelanomaCITResponse_scRNAseq_TILandPBMC_publication. Any additional information required to reanalyze the data reported in this paper is available from the lead contact upon request.

EXPERIMENTAL MODEL AND STUDY PARTICIPANT DETAILS

Patient samples
Cryopreserved peripheral blood mononuclear cells (PBMCs) and freshly resected tumor specimens of stage III-IV treatment-naive melanoma patients were provided by the Department of Dermatology, University Hospital Zurich, Switzerland. All patients received CPI therapy after surgery (Table S1). All human biological samples were collected after written informed consent from patients was obtained and with approval of the local ethics committee (Kantonale Ethikkommission Zürich, KEK-ZH authorization BASEC2017-00494, and BASEC2014-0425) in accordance with the Declaration of Helsinki.

Progression was defined as measurable increase in tumor volume, the presence of new metastatic sites or the need to treat the patient with a secondary treatment such as radiotherapy. In the adjuvant setting, responders were defined as continuing being tumor-free (TF) at 6 months after treatment initiation.

In Table S1 we report all sample information. Data on socioeconomic status, ethnicity and ancestry were not collected.

METHOD DETAILS

Tumor dissociation
Tumor lesions were mechanically dissociated and digested using accutase (PAA), collagenase IV (Worthington), hyaluronidase (Sigma), and DNAse type IV (Sigma). Single-cell suspensions were stored in liquid nitrogen until further usage.

Flow cytometry

Cryopreserved tumor digests from melanoma samples, as well as autologous PBMCs were thawed and washed with excess ice-cold 1xPBS and spun down at 350xg for 5 min. Subsequently, the cells were stained with Live/Dead (APC-Cy7 (Near IR), Thermo Fisher Scientific, #L34976) and anti-human CD45 (FITC, Biolegend, #304006) in presence of Fc block (Biolegend #422302), and large debris were removed with a 40-μm strainer (pluriSelect, #43-10040-40). All samples were acquired on the BD FACS ARIA Fusion III (Becton Dickinson GmbH, Germany). For scRNA-seq experiments, live and single gated cells were sorted into non-immune cell (CD45$^-$) and immune cell (CD45$^+$) populations. Both populations were directly sorted into Eppendorf tubes with 1xPBS supplemented with 1% BSA for scRNA-seq.

Tumor mutational burden measurements

Tumor mutational burden (TMB) was measured in tumor tissue using the comprehensive genomic profiling test from Foundation medicine (Roche) and reported as mutations per megabase (Mts/Mb).

Single cell RNA-sequencing

For all samples, scRNA-seq was performed using Chromium Single Cell 3′ GEM, Library & Gel Bead Kit v2 (10x Genomics, Pleasanton, CA, USA) following the manufacturer's protocol. Briefly, 10000 CD45$^+$ immune cells per sample, diluted at a density of 100–800 cells/μl in PBS plus 1% BSA (determined by Cellometer Auto 2000 Cell Viability Counter (Nexcelom Bioscience, Lawrence, MA USA)), were loaded into the 10x Chromium Controller and library preparation was performed according to the manufacturer's indications (Chromium Single Cell 3′ Library & Gel Bead Kit v2, i7 Multiplex Kit, Single Cell A Chip (all 10x Genomics), SPRIselect Reagent Kit (Beckman-Coulter)). The quality and concentration of both cDNA and libraries were assessed using an Agilent BioAnalyzer with High Sensitivity kit (both Agilent, Santa Clara, CA USA) and Qubit Fluorometer with dsDNA HS assay kit (both Thermo Fisher Scientific, Waltham, MA USA) according to the manufacturer's recommendation.

The samples were mixed equimolarly and the libraries were clustered using an Illumina cBOT instrument (HiSeq 3000/4000 PE Cluster Kit) and sequenced on an Illumina HiSeq 4000 (HiSeq 3000/4000 SBS Kit, 150 cycles) with a depth of ∼50,000 reads/cell and the recommended read configuration (R1 = 28, I7 = 8 and R2 = 91). The output files were converted to FASTQ files using the Cell Ranger pipeline.

QUANTIFICATION AND STATISTICAL ANALYSIS

Single cell RNA-sequencing data processing

Fastq files were aligned to the human transcriptome (hg19) using 10x Genomics Cell Ranger count (Version 2.1.1) with the parameters "–expect-cells = 6000" and velocyto 0.17 was used to quantify spliced versus unspliced reads. We obtained on average 33% of unspliced reads across all samples. All cells showing expression of >200 genes were further merged across all samples and processed with besca's 2.4 standard workflow, cell annotation workflow and with scanpy 1.4.5.[103,104] Filtering was performed with the parameters min_genes = 500, min_cells = 10, min_counts = 1000, n_genes = 8000, percent_mito = 0.15; max_counts = 60000. In brief, RNA counts were normalized per 10k, the top highly variable genes were selected per sample (parameters 'batch_key = experiment'), total gene and mitochondrial reads were regressed out, a Principal component analysis (PCA) was performed, and the first 50 principal components (PCs) were used for nearest neighbor calculations and Leiden clustering (resolution = 3),[111] as well as for uniform manifold

approximation and projection (UMAP)-based visualization. Cell annotation was performed using besca's cell annotation workflow and the sig-annot module (cell type markers are listed in Table S2), with the nomenclature following cell ontology (CL) conventions wherever possible (e.g., "CD141-positive myeloid dendritic cell" for cDC1).[112] After an initial, global analysis, myeloid cells, T cells, PBMC-derived and tumor-infiltrated immune cells were reanalysed and annotated separately and the final annotation obtained from manual integration of all analysis versions. For the downstream analyses (differential abundance and differential expression across response classes) patients 12 and 38 were excluded as CPI-treatment was given one year post surgery and CPI-treatment was given for one injection only, respectively. The PBMC samples of patients 67, 68, and 87 were excluded from the response analysis as they were collected after treatment administration; additionally, for patients 79, 64, and 67, which had 2 (either biological or technical) replicates per patient, we only selected a single one, retaining those with larger cell number, lower dropout rate, lower overall mitochondrial percentage, and/or higher sequencing depth.

Trajectory and velocity analysis

Toward the CD8$^+$ T cell velocity analysis, all cells annotated as "CD8-positive T cells", excluding NK-like T cells, were considered. Bbknn[105] was applied using the patient ID as batch, followed by calculation of diffusion maps (default parameters; n = 15), nearest neighbors (n = 15) based on the diffusion components, Leiden clustering (resolution = 0.5), PAGA[113] (default parameters), and finally PAGA-initiated UMAP for visualization. As clusters 2 and 4 were primarily derived from a single patient (Figure S6E) and clusters 12 and 14 consisted primarily of proliferating cells in the G2M phase, we excluded them from the velocity analyses described in Figures 5 and 6. We used scanpy 1.6 and scvelo 0.2.2 in dynamical mode to estimate cellular velocities (direction and speed of individual cells in gene expression space), cellrank 1.0.0 to estimate most likely initial and terminal states and subsequently set the root cell for latent time (a measure indicative of a cell's internal clock) estimates. For visualisation, velocity vectors were projected on the UMAP in a streamline plot, where similarly directed vectors are connected. Finally, based on RNA velocities and transcriptomic similarity we calculated directed PAGA graphs (parameters root_key = 'initial_states_probs', end_key = 'terminal_states_probs', use_time_prior = 'velocity_pseudotime') to estimate and visualize most likely transitions across cell clusters/states. We first performed a joint analysis, which included all samples (Figure 5), and subsequently we analyzed R + TF and NR samples separately (Figure 6), either across all clusters or only focusing on subpaths of interest - cluster 15, 13, 8, 0, and 11 for the tumor-tumor path and clusters 9, 0, 11, 5, and 6 for the PBMC-tumor path. Per population of interest and responder population we identified putative velocity driver genes by using cellrank's "lineage_drivers" function (cutoff = 0.1). Full results are listed in Table S6. Genes displayed in Figure 6C contain a subset of such lineage drivers which are also estimated to be differentially expressed across CD8$^+$ T cell populations. To generate Figure 6E, we used bins of size = 0.05 across latent time values (0–1) and visualized expression (log_cp10k) across R and NR cells falling inside the respective bins. Latent time values across clusters and response classes were averaged across all cells of a group and sample and compared across samples using a Wilcoxon rank-sum test.

Monocyte/macrophage velocity analysis was performed similarly. We first used all cells annotated as 'macrophage', 'classical monocyte' and 'non-classical monocyte', applied bbknn (batch_key = patientID), calculated diffusion maps (default, n = 15), nearest neighbors based on diffusion components (n = 10), Leiden clustering

🧬 **CellPress**

(resolution = 0.75), PAGA (default parameters), and PAGA-initiated UMAP for visualization. We subsequently only retained clusters annotated as MSR1, CXCL9, and MARCO-positive macrophages (14, 16, 19, 2, 23, 7, 13, and 7), as well as classical monocyte clusters directly transitioning into the macrophage clusters (5, 29, 12). We used scanpy 1.6 and scvelo 0.2.2 in dynamical mode to estimate cellular velocities, cellrank 1.0.0 to estimate most likely initial and terminal states and subsequently set the root cell for latent time estimates. For visualisation, velocity vectors were projected on the UMAP in a streamline plot, where similarly directed vectors are connected. Finally, based on RNA velocities and transcriptomic similarity we calculated directed PAGA graphs (parameters root_key = 'initial_states_probs', end_key = 'terminal_states_probs', use_time_prior = 'velocity_pseudotime') to estimate and visualize most likely transitions across cell clusters/states. We first performed a joint analysis, which included all samples (not shown), and subsequently we analyzed R + TF and NR samples separately (Figure 2G).

For the CD4$^+$ T cell analysis, we first used all cells annotated as CD4$^+$ T cell, applied bbknn (batch_key = patientID), calculated diffusion maps (default, n = 15), nearest neighbors based on diffusion components (n = 10), Leiden clustering (resolution = 0.25), PAGA (default parameters), and PAGA-initiated UMAP for visualization. We subsequently removed 2 regulatory T cell and 2 naive cell clusters, retaining memory/effector and proliferating populations (clusters 0, 1, 2, 5, 6, 8, 9, 10, 11, 13). We used scanpy 1.9.4 and scvelo 0.2.5 in dynamical mode to estimate velocities. For visualisation, velocity vectors were projected on the UMAP in a streamline plot, where similarly directed vectors are connected. Finally, based on RNA velocities and transcriptomic similarity we calculated directed PAGA graphs (parameters root_key = 'iroot', end_key = 'iroot', use_time_prior = 'velocity_pseudotime') to estimate and visualize most likely transitions across cell clusters/states. We first performed a joint analysis, which included all samples (Figure 4C). We further analyzed R + TF and NR samples separately (Figure 4D). We exported genes listed as putative velocity drivers (velocity_genes = True) in R/TF or NRs, respectively to Table S6 and displayed those with a fit_likelihood >0.1 in the respective patient group (R/TF or NR) that were also differentially expressed in at least one CD4$^+$ T cell subset in Figure 4D.

Cell-cell interaction analysis

Cell-cell interaction analysis was performed using cellphonedb v2.0.0 with default parameters across all identified tumor immune subsets, per patient. Estimated significant interactions ("significant_means") involving either monocyte/macrophage or cDC subsets and T/NK subsets were filtered based on the frequency of interactions in R/TF compared to NR as well as the expression patterns of the genes involved in the interactions. In brief, we started with all interactions predicted in at least two patients among a set of cell types of interest. Next, for each cell population of interest (monocyte-macrophage or myeloid dendritic cell subtype), we only considered interactions involving a gene that was enriched compared to all other cells (one-versus-all Wilcoxon rank-sum test, cutoffs fold-change 1.5 and adjusted p value 0.1). We further removed interactions that were not predicted to occur in at least half of either R or NR patients. We did not take into account the strength of the predicted interaction, but contrasted the occurrence of the interactions in the R/TF versus the NR patients using Fisher's exact test (per cell type pair), further removing all predicted interactions with p>=0.3. We further filtered these interactions to those with the abs(max(abs(log10(RvsNR_ratio))) - min(abs(log10(RvsNR_ratio))))>1.25 (for DC, which had fewer interactions) or 1.75 (for monocytes/macrophages, which had more interactions) as well as max(abs(log10(ratio)))>1.5, which

we displayed in Figures 3A and 3B. When looking at intersections with the differentially expressed genes, all the interactions prior to the RvsNR_ratio filtering were considered.

Differential cell abundance

For comparing cell abundances between R and NR patients in tumors and PBMCs, respectively, we used a generalized linear mixed effects model approach as described previously,[114] using the lme4 R library, treating each patient (sample) as a random effect and adding the total counts per cell type as additional weights.[110] We performed both a separate analysis per adjuvance class and a joint analysis, where (R + TF) were compared to all NR, while factoring adjuvance into the model (glmer(count/total_count ~ cell_type + Adjuvant +(1 | PatientID), weights = total_count, family = 'binomial')). Full results of all comparisons are available in Table S3. The three PBMC samples collected after the treatment were excluded from the comparison. All other cell abundance comparisons were performed using a Wilcoxon rank-sum test.

Differential expression analysis

Differential expression (DE) analysis was performed per specified cell subset at cell level using a Wilcoxon rank-sum test, the fold-change of 2 (cluster comparison) or 1.5 (response comparison) and the adjusted p-value cutoff of 0.05 (cluster comparison) or 0.1 (response comparison). For the response comparison, we performed several analyses: (1) on all data, when R + TF cells were contrasted to NR cells across lesions and adjuvance classes; (2) separately on LN, brain and other (all other lesion types) samples; (3) separately on adjuvant and non-adjuvant patient samples. All significant DE results, including the specific cutoff used, are available in Table S4. In Figure 2I only genes showing significant differential expression across both adjuvance classes (separate adjuvant and non-adjuvant comparisons) and lymph-node only in addition to the global comparison were included. In Figure 3D (top) we included only a subset genes showing significant differential expression in at least 4 subsets of interests (cytokine-secreting, EM, exhausted-like, NK-like, proliferating CD8$^+$ T cells, CD56-bright, CD56-dim NK cells, or all CD8$^+$ T and NK cells), with significant differences stable across both adjuvance classes (separate adjuvant and non-adjuvant comparisons) and lesions (LN and brain/others separately) in at least one of the subsets. For CD4$^+$ T cells (Figure 3D, bottom), we included genes significantly differentially expressed in at least 2 subsets of interest, with significant differences stable across both adjuvance classes and lesions in at least one of the subsets.

Pathway enrichment analysis

Pathway enrichment analysis was performed using gseapy enrichr[106,115] module for the analysis at the single-cell level, using the top 200 differentially expressed genes (when available) and all genes showing a mean log(cp10k) expression >0.01 in the respective cell subset of interest as background. All results are listed in Table S5. Displayed signature scores represent the natural log of the p-value multiplied by the Z score. For Figures 2K and 3E, we only included pathways with a combined score >20 (in any comparison), and further filtered for pathways with an absolute combined score difference (R vs. NR) > 10 in both monocytes and macrophages (Figure 2K); cytokine-secreting, effector-memory, or exhausted-like CD8$^+$ T cells (Figure 3E), or naive and central-memory, effector-memory, effector and exhausted-like, or all CD4$^+$ T cells (Figure S4C), respectively.

Pseudo-bulk analysis

For the pseudobulk analysis (Figures 1E and S2B–S2E), we summed expression values across all cells belonging to a sample across all tumor-derived immune cells

using besca's pseudobulk function. The subsequent analysis was performed in R,[116] using the packages edgeR,[107] vsn,[108] Hmisc, and camera.[109] In brief, genes were further filtered to have at least as many non-zero samples per gene as the number of samples in the main groups. Additionally, only genes with above median expression in samples with <50% zero counts were retained. Data was normalized using edgeR's calcNormFactors function (default parameters) and variance stabilization (vsn), and a principal component (PC) analysis was performed (prcomp function). Spearman correlations of the top three PCs with the experimental variables were calculated using Hmiscrcorr and analyzed. The following experimental covariates showed at least 20% correlation and p-value < 0.05: mutation status (PC1), cell_subtype (PC2), response (PC3), adjuvance class (PC3) and library size (PC3). We next performed a differential expression analysis using the edgeR package, followed by a pathway enrichment analysis using the camera algorithm, contrasting either BRAF to NRAS samples (mutation comparison) or lymph node to brain and other samples, respectively (lesion comparison).

Other scRNA-seq related analyses

Downstream analyses and further plotting were performed using scanpy 1.6 and 1.9.5. Signature enrichment at single cell level was performed using scanpy's score_genes method with default parameters. All employed signatures are listed in Table S2.